LITHOSPHERE (RUSSIA), 2018, volume 18, No. 5A, pp. 57–77

XENOCRYSTS AND MEGACRYSTS OF ALKALINE OLIVINE-BASALT-BASANITE-NEPHELINITE ASSOCIATION MAKHTESH RAMON (ISRAEL): INTERACTION WITH CARRIER MAGMAS AND CRYSTALLOGRAPHIC TRANSFORMATIONS

Zinovi Yudalevich, Yevgeny Vapnik

Department of Geological and Environmental Sciences, Ben-Gurion University of the Negev, P.O.B. 653, Beer-Sheva, 84105 Israel, e-mails: zinovi@bgu.ac.il, vapnik@bgu.ac.il

Received 19.01.2018, accepted 15.02.2018

The article considers xenocrysts and megacrysts hosted in the rocks of Early Cretaceous olivine-basalt-basanite-nephelinite association that outcropped in the erosion crater of Makhtesh Ramon (Natural Reserve of Mishmar ha-Nagev, Israel). This magmatic rock association contains a wide spectrum of xenoliths trapped at different crustal levels. These are upper mantle, lower and upper crustal xenoliths. Mantle xenoliths are represented by peridotites, olivine clinopyroxenites, clinopyroxenites, olivine websterites, websterites and their amphibole-bearing analogues. Lower crustal xenoliths are mafic granulites, such as metagabbros and plagioclasites, whereas upper crustal xenoliths are the fragments of Neoproterozoic tuffs. Xenocrysts and megacrysts are the fragments of xenoliths that chipped from them on their way to the surface. Alterations in xenoliths, xenocrysts and megacrysts caused by the host melt constitute a common petrographic feature. Xenocrysts and megacrysts are mainly represented by minerals that are compatible with the magmatic rock association. These are olivine, clinopyroxene, amphibole, nepheline, plagioclase, anorthoclase, apatite, magnetite and spinel. The xenocrysts of quartz and orthopyroxene are incompatible with the SiO_2-undersaturated host rock of this magmatic association. Main reasons determining the interaction between magma and xenoliths include rapid decompression, metamorphism and metasomatism. Xenocrysts are subjected to metamorphism that corresponds to high-temperature facies of contact metamorphism, up to the partial melting of xenocrysts. Metasomatism is directed at equalising the compositions of xenocrysts and eponymous minerals that crystallised from the host melt. There are several important criteria adopted to identify xenocrysts and distinguish them from phenocrysts. These are partial melting, solid-phase decomposition, decrystallisation of primary (before-trapping) textures, recrystallisation and self-faceting of initially xenomorphic grains into the crystals with perfect habits. The chemical composition of xenocrysts has mineral and geochemical indications of xenogenic origin, as well as the signs of a newly-formed substance.

Keywords: *melting, solid-phase decomposition, decrystallisation, self-faceting, xenocrysts, megacrysts, xenoliths, magmatic rocks, Makhtesh Ramon, Israel*

Acknowledgments

The authors express their gratitude to Prof. M. Eyal (Ben-Gurion University, Beer-Sheva, Israel), who was responsible for the overall management of works on studying the magmatism of Makhtesh Ramon. The authors are thankful to O. Dvir (Hebrew University of Jerusalem), V.V. Hiller (IGG UB RAS, Russia), Prof. Ya. Kazir and Ph. students B. Elisha, Ts. Golan, I. Gendelman (Ben-Gurion University, Israel) for the assistance in studying chemical compositions of minerals; Dr. R. Granot (Ben-Gurion University) for providing new data on the Ar-Ar-ages of the studied rocks. The authors are grateful to Prof. G.B. Fershtater (IGG UB RAS, Russia) for comprehensive consultations on petrological issues associated with the study of deep-seated xenoliths and xenocrysts.

INTRODUCTION

During their rise to the earth's surface and under decompression, xenoliths disintegrate, decompose into monomineral fragments (xenocrysts and megacrysts) and enter into a geochemical interaction with the carrier melt, get partially or completely absorbed by it, thus becoming a part of a single magmatic system. In terms of shape and size, xenocrysts and megacrysts, as a rule, externally resemble phenocrysts and their identification constitutes an urgent petrological task.

The present article examines the petrographic and geochemical features of xenocrysts and megacrysts widely developed in the igneous rocks of Makhtesh Ramon, as well as demonstrates the similarities between changes occurring in them and transformations in xenoliths. Special attention is paid to the morphological tendency of initially xenomorphic xenocrysts and megacrysts to take crystallographically regular forms, which complicates their identification as minerals alien to the host rocks.

GENERAL GEOLOGICAL DATA ON THE AREA

Tectonically, the area belongs to the territory of the Levant – the continental margin of the Eastern Mediterranean, in the east limited by the transform fault of the Dead Sea, within which the rocks of the Proterozoic crystalline basement are overlain by a thick cover of Meso-Cenozoic deposits.

Makhtesh Ramon constitutes a sublatitudinal mountain depression (45 km long and 10 km wide), whose formation is explained by the erosion of a large

anticline having gently sloping northern and steeply falling southern wings during the formation of the Syrian Arc echoing the collision of the African and Arabian plates with the Alpine-Himalayan orogenic belt in the Late Cretaceous. The stratigraphic cross section of the area up to a depth of more than 1 km is represented by Middle and Upper Triassic deposits (Gevanim, Saharonim and Mohilla FMS: limestones, marls, sandstones, gypsums), Lower and Middle Jurassic deposits (Mishor, Ardon, Inmar и Mahmal FMS: laterites, limestones, dolomites, marls, sandstones, clays), as well as Lower and Upper Cretaceous deposits (Arodcgl + Lower Hatira Fm + Upper Hatira Fm, Hazera, Sayarim и Mishash FMS): conglomerates, sandstones, marls, clays, silicas) (Fig. 1). Two long intervals between sedimentation were established: 1. the Upper Triassic – beginning of the Jurassic; 2. the Upper Jurassic – the Lower Cretaceous (up through and including the Barremian Stage). Clearly, the Late Triassic and Early Cretaceous magmatic activities in the area resulted in the tectonic activity, which coincided in time with these breaks.

GEOLOGICAL, PETROGRAPHIC AND GEOCHEMICAL FEATURES EXHIBITED BY IGNEOUS ROCKS IN THE AREA

Basic data on the age, composition, as well as the geodynamic regime for the formation of magmatites in the area were considered in [Garfunkel, Katz, 1967; Bonen et al., 1980; Lang, Steinitz, 1989; Baer et al., 1995; Eyal et al., 1996; Samoilov, Vapnik, 2005; Vapnik et al., 2007; Yudalevich et al., 2014]. As a result, one Triassic and two Early Cretaceous associations manifested in the form of lava flows and small intrusions (sills, laccoliths and dykes) were identified. The Triassic Saharonim Association is represented by alkaline olivine basalts (K-Ar age of 213.6 Ma, Upper Triassic, Norian Stage) and is chronologically associated with the pre-Jurassic stage of laterite formation Mishor Fm. Early Cretaceous magmatites are divided into two rock groups: 1) an early bimodal group composed mainly of alkaline basalts, gabbro and syenites (K-Ar age of 129–140 Ma, Early Cretaceous, Valanginian – Barremian stages); 2) a later group made up of olivine, basalt, basanite and nephelinite (Ar-Ar age of 112.9–119.0 Ma, Early Cretaceous, Aptian stage).

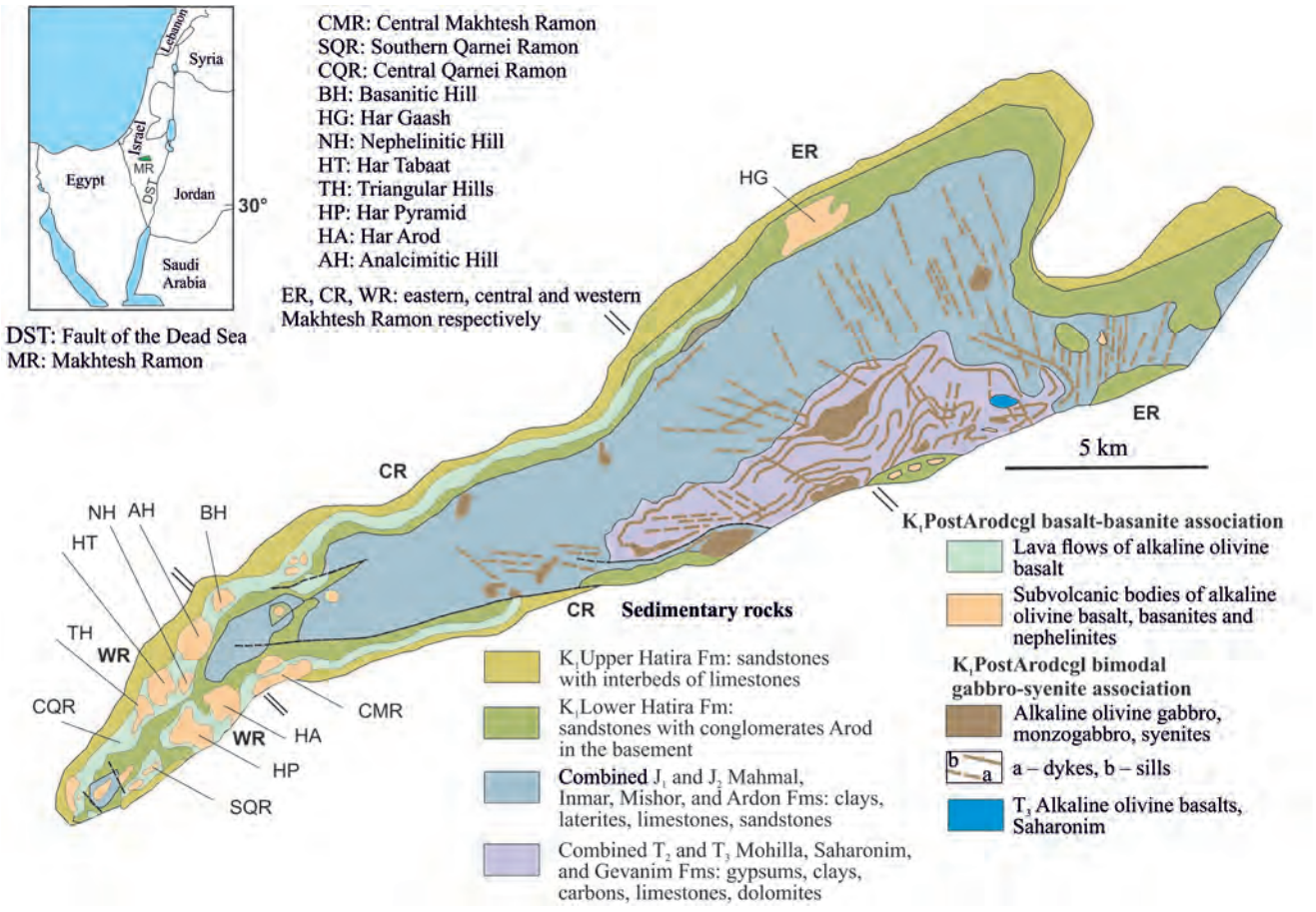

Fig. 1. Location and a schematic geological map of Makhtesh Ramon.

Cretaceous associations identified using radiological data reveal geological evidence of their different ages: the earlier one is overlain by Arod conglomerates lying at the base of Lower Hatira Fm, i.e. it is pre-conglomerate – PreArodcgl. However, the rocks of the later association overlie and intrude these conglomerates, as well as Lower Hatira Fm sandstones occurring above, i.e. they are post-conglomerate – PostArodcgl. In turn, the sandstones of Upper Hatira Fm rest erosively on magmatites, thus fixing their geological age between Lower and Upper Hatira Fms.

All magmatic manifestations in the area belong to one OIB-like alkaline geochemical type.

Xenoliths and xenocrysts have not been found in the Triassic and Early Cretaceous associations yet; however, they are widely developed in the PostArodcgl group, which is the most complex in terms of internal structure and composition. It comprises lava flows, tuffaceous and tuffaceous-sedimentary deposits, pyroclastic diatremes, subvolcanic stocks, dykes and sills. The association is represented by olivine basalts and microgabbros, basanites, nephelinites, as well as their melilite and analcime variations, often containing volcanic glass. All the rocks are of black, dark green or green-grey colour, porphyritic texture and are practically indistinguishable in composition under field conditions. The inclusions of olivine and clinopyroxene are of cross-cutting nature; in addition, plagioclase phenocrysts are found in basalts, and melilite phenocrysts are observed in nephelinites. Their number ranges from 5–8 to 34%, with their size varying from 0.6 mm to 2.0 cm. The bulk of basalts and basanites are composed of olivine, clinopyroxene and plagioclase, calcite, micromicaceous or pelitomorphic minerals such as chlorophaeite and saponite, nepheline and analcime (in basanites), as well as melilite (in the foidite group), excluding plagioclase.

There are deep-seated (mantle and lower crustal) and upper crustal xenoliths (tuffs of the Proterozoic base, sedimentary cover rocks). Deep-seated xenoliths are characterised in [Bonen et al., 1980; Stein, Katz, 1989; Vapnik, 2005], while a more complete list of them, including lower crustal ones, is given in [Fershtater et al., 2016; Fershtater, Yudalevich, 2017]. These studies examined primarily the interaction between xenoliths and host melts at a deep-seated mantle-lower crustal level.

The present study is aimed at studying phenomena occurring in xeno- and megacrysts during uplift and decompression, which takes them to the magma surface, as well as associated mineralogical, petrochemical and morphological transformations.

The deep-seated xenoliths of the PostArodcgl association are represented by mantle dunites, harzburgites, lherzolites, wehrlites, olivine clinopyroxenites and clinopyroxenites, olivine websterites, websterites and their amphibolite varieties, lower-crustal metagabbros (granulites), apatite-magnetite and clinopyroxene-apatite-magnetite rocks. In addition to the deep-seated xenoliths, there are xenoliths of Late Proterozoic tuffs.

Along with xenoliths, xeno- and megacrysts are widespread in rocks. A common petrographic feature of xenoliths, xeno- and megacrysts are alterations caused by the host melts and minerals in the late stage of their crystallisation, represented by oligoclase-andesine, potassium feldspar, clinopyroxene, titanomagnetite, apatite, biotite, rhonite, calcites, zeolites and saponite-chlorophaeites.

Xeno- and megacrysts are genetically similar formations and differ only in size. They constitute fragments of xenoliths, which appear in the course of transporting xenoliths to the magma stabilisation sites. Xenocrysts are close to phenocrysts in size and usually do not exceed 1.2 mm, whereas megacrysts are much larger and reach 15.0 cm across.

ANALYTICAL STUDIES

The compositions of minerals given in the tables were determined using a CAMECA SX-100 microanalyser at the Institute of Geology and Geochemistry UB RAS (Ekaterinburg, operator V.V. Hiller), Institute of Geology SB RAS (Novosibirsk, V.V. Sharygin), as well as using a JEOL microanalyser (ISP-MS and ERMA) at the Hebrew University of Jerusalem (analyst O. Dvir).

CHARACTERISTICS OF XENOCHRYSTS

Xeno- and megacrysts differ from phenocrysts in the following characteristics: 1 – xenomorphic (porphyroclastic) outlines and the development of near-contact corrosion; 2 – rock jointing, optical defects and decrystallisation; 3 – the diffuse effect of host magma; 4 – melting and formation of decomposition structures; 5 – non-conformity with the paragenesis of host rocks (‘prohibited’ minerals). The bulk of xeno- and megacrysts are represented by compatible minerals, with only the xenocrysts of quartz and orthopyroxene being incompatible with the host rocks undersaturated with SiO_2.

Quartz. The size of the xenocrysts varies from 0.2 mm to 1.2 mm, with their shape being round or oval. It is usually surrounded by a clinopyroxene rim made up of the smallest adjacent and optically differently oriented microlites having a tendency to form a regular pyroxene form, common to the entire rim. The intergranular gaps in the rim are filled with dark brown glass of orthoclase composition. At the border with the pyroxene rim, quartz is often melted into yellow or greenish-brown glass (Fig. 2a) enriched with MgO (35.56–36.37 wt %). The difference in the composition of the glasses is given in Table 1. Sometimes quartz undergoes decrystallisation with a polymorphic transition to tridymite and cristobalite. On

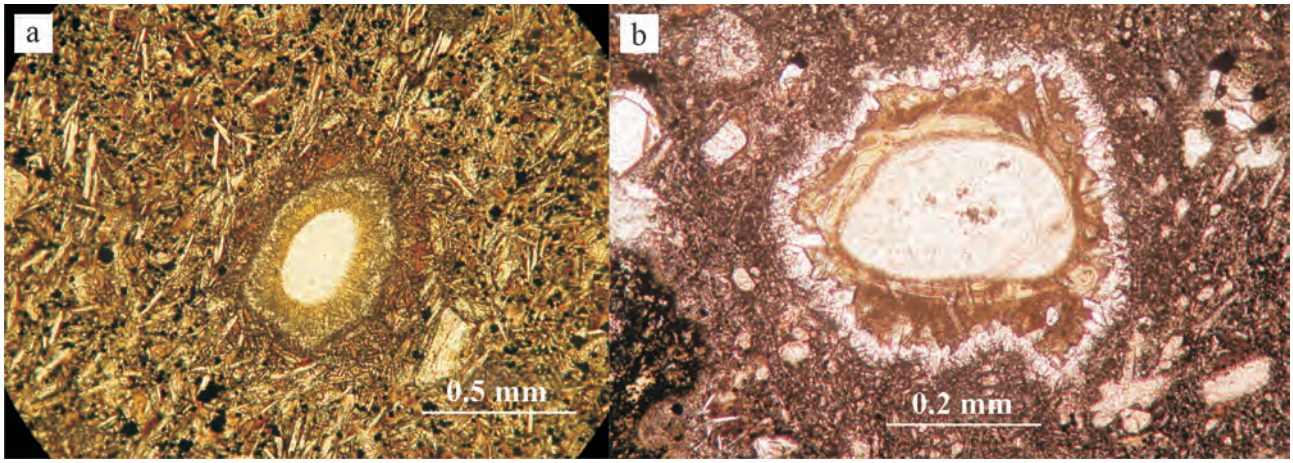

Fig. 2. Quartz xenocrysts and products of their alteration.

a – BH-16 (olivine basalt) and b – CMR-178 (nephelinite). Quartz xenocryst transitioned into fine-grained tridymite-cristobalite aggregate with the melting zone being composed of greenish-brown glass and light green saponite. The outer zone is composed of microlitic clinopyroxene. PPL.

Table 1. Chemical composition of xenocrysts and products of their alteration, wt %

		SiO_2	TiO_2	Al_2O_3	Cr_2O_3	FeO	MnO	MgO	CaO	Na_2O	K_2O	Total	Mg*	*An*
Products of quartz alteration	1(3)	61.86	–	1.96	–	–	–	35.98	0.2	–	–	100	–	
	2(3)	54.2	–	–	–	6.59	–	16.35	22.59	0.77	–	100	0.85	
	3(1)	65.34	–	14.26	–	4.83	–	0.73	–	2.01	12.81	99.98	–	
	4(1)	43.87	4.28	9.72	–	7.55	–	11.97	21.62	0.98	–	99.99	0.78	
Orthopyroxene and products of its alteration	1(2)	54.41	–	4.2	–	5.93	–	34.57	–	–	–	99.11	0.93	
	2(1)	47.91	–	5.39	–	8.49	–	32.07	5.41	–	–	92.27	0.73	
	3(1)	38.95	–	2.41	–	24.16	–	33.38	0.66	–	0.44	100	0.76	
	4(2)	51.92	–	2.76	–	9.51	–	13.76	19.62	1.94	–	99.51	0.76	
	5(1)	51.96	0.14	1.98	–	21.62	0.52	21.45	1.1	0.04	–	98.81	0.7	
	6(4)	36.55	–	–	–	30.72	–	30.77	0.26	–	–	98.3	0.7	
	7(1)	34.98	–	–	–	40.1	–	23.41	0.2	–	–	98.69	0.57	
	8(4)	52.98	0.5	0.59	0.07	10.63	–	14.72	18.29	0.93	–	98.71	0.76	
	9(1)	50.93	0.29	2.94	–	13.33	–	11.54	19.7	0.68	–	99.41	0.66	
	10(43)	54.59	–	3.43	0.26	6.77	–	33.73	0.89	–	–	99.67	0.92	
	11(7)	51.43	0.15	1.83	0.04	24.91	0.59	19.27	1.12	0.07	0.01	99.45	0.64	
Olivine	1(3)	40.93	0.03	–	–	10.8	0.18	47.35	0.13	–	–	99.42	0.91	
	2(2)	39.07	0.05	0.06	–	20.47	0.54	39.59	0.32	–	–	100.1	0.82	
	3(1)	40.12	–	–	–	14.8	–	44.33	0.18	–	–	99.43	0.87	
	4(1)	39.2	–	–	–	19.76	–	41.04	–	–	–	100	0.83	
	5(2)	38.15	–	–	–	24.84	–	36.57	0.45	–	–	100.01	0.77	
	6(1)	38.11	–	–	–	24.32	–	37.62	–	–	–	100.05	0.78	
	7(10)	37.33	0.02	0.04	–	26.19	0.44	35.11	0.42	–	–	99.55	0.75	
	8(19)	39.18	–	–	–	19.06	0.37	40.99	0.34	–	–	99.94	0.83	
Clinopyroxene	1(1)	50.36	1.19	4.45	0.74	3.74	–	14.56	24.22	0.51	–	99.77	0.9	
	2(2)	44.77	3.56	8.11	0.51	6.84	–	12.3	23.08	0.83	–	100	0.8	
	3(2)	50.7	0.68	5.52	0.93	4.14	–	16.37	20.95	1.09	–	100.38	0.9	
	4(1)	47.51	2.07	6.37	–	7.17	0.14	13.36	22.96	0.42	–	100	0.81	
	5(49)	44.27	3.86	8.13	–	8.13	0.12	11.08	23.16	0.47	0.11	99.33	0.76	
	6(15)	44.44	3.88	9.64	–	6.22	0.21	12.33	21.61	0.79	–	99.12	0.82	

Table 1. Ending

		SiO_2	TiO_2	Al_2O_3	Cr_2O_3	FeO	MnO	MgO	CaO	Na_2O	K_2O	Total	Mg*	*An*
Amphibole and products of its alteration	1(1)	39.35	7.93	11.98	–	12.27	–	12.86	13.98	2.06	0.57	101	0.71	–
	2(9)	25.41	11.88	16.46	–	20.24	–	12.73	11.71	1.57	–	100	0.59	–
	3(3)	38.49	–	–	–	24.08	–	36.85	0.61	–	–	100.03	0.78	–
	4(3)	44.82	4.09	8.23	–	6.01	–	12.84	23.26	0.75	–	100	0.83	–
	5(3)	52.81	–	29.86	–	–	–	–	–	12.29	5.04	–	–	57
	6(9)	40.15	5.81	13.31	–	9.88	0.19	12.29	11.91	2.49	1.05	97.08	0.74	–
	7(5)	25.79	10.62	16.92	–	18.93	–	13.75	11.78	1.72	–	99.51	0.62	–
	8(6)	41.42	1.57	13.19	0.39	9.05	0.08	16.16	10.84	2.91	0.86	96.47	0.8	–
	9(11)	40.12	4.83	13.54	–	10.11	0.11	12.18	11.97	2.18	2.04	97.08	0.75	–
	10(5)	24.96	11.96	18.18	–	13.22	0.7	15.86	10.04	1.6	–	96.52	0.73	–
	11(4)	25.11	11.05	13.64	–	26.21	0.24	10.61	11.07	1.47	–	–	0.48	–
Plagioclase	1(4)	53.67	0.32	27.98	–	0.81	0.04	0.21	10.45	4.97	0.58	99.03	–	54
	2(2)	51.85	–	30.25	–	–	–	–	12.93	4.38	0.59	100	–	61
	3(2)	54.35	0.25	27.14	–	0.84	0.05	0.67	9.95	7.01	0.73	100.99	–	44
	4(1)	50.79	–	30.34	–	–	–	–	14.77	3.61	0.49	100	–	68
	5(2)	54.87	–	28.19	–	0.56	–	0.01	11.16	5.3	0.22	100.31	–	54
	6(7)	51.55	–	30.38	–	–	–	–	12.95	4.51	0.61	100	–	67

		SiO_2	TiO_2	Al_2O_3	Cr_2O_3	FeO	MnO	MgO	CaO	Na_2O	P_2O_5	F	Cl	Total
Magnetite and spinel	1(3)	–	14.94	4.8	–	77.84	–	2.43	–	–	–	–	–	100.01
	2(1)	–	20.83	5.76	–	70.9	–	2.51	–	–	–	–	–	100
	3(63)	0.04	21.46	6.43	0.51	63.89	0.85	4.77	0.12	–	–	–	–	98.07
	4(1)	0.03	10.27	13.54	7.81	57.85	0.37	6.95	0.06	–	–	–	–	96.88
	5(1)	–	0.83	38.01	25.14	19.26	0.13	15.47	–	–	–	–	–	98.84
	6(1)	0.02	17.22	7.58	3.66	63.26	0.6	4.86	0.08	–	–	–	–	97.28
	7(1)	–	–	63.34	–	13.27	–	23.39	–	–	–	–	–	100
	8(1)	–	15.38	10.42	–	67.06	0.8	6.08	0.02	0.24	–	–	–	100
Apatite	1(3)	–	–	–	–	0.59	–	–	53.49	0.36	41.18	3.77	0.61	100
	2(6)	–	–	–	–	–	0.13	–	52.33	–	40.93	6.17	0.44	100

Note. The number of analyses involved in the calculation of average contents is given in parentheses after the sequence number.
Alteration products of quartz xenocrysts: HP-6G: 1 – moderate yellow green glass at the periphery of quartz, 2 – fine-grained clinopyroxene at the outer border of glass, 3 – dusky red glass filling the interstices between the fine grains of clinopyroxene, 4 – clinopyroxene from host basanite matrix.
Chemical composition of orthopyroxene xenocrysts and products of their alteration: BP-14G: 1 – xenocryst of lherzolite type, core; 2 – rim adjacent to the zone of decomposition, products of orthopyroxene decomposition: 3 – olivine, 4 – clinopyroxene. TH-16: 5 – xenocryst of gabbro type; products of xenocryst decomposition: 6–7 – olivine, 8–9 – clinopyroxene. Orthopyroxene from xenoliths: 10 – lherzolite type, 11 – gabbro type.
Chemical composition of olivine: NH-596: 1 – megacryst, core, 2 – rim. BP-1G: 3 – megacryst, core, 4 – intermediate zone, 5 – rim, 6 – zone of megacryst decrystallisation. 7–8 – olivine from host magmatic rocks: 7 – prismatic microphenocrysts in rock matrix, 8 – melt inclusions hosted in the olivine and clinopyroxene of peridotites.
Chemical composition of clinopyroxene xenocrysts: BH-11: 1– xenocrysts, core. BH-1G: 2– rim. HP-10G: 3 – megacryst, core, 4 – rim. 5 – prismatic microphenocrysts in rock matrix, 6 – melt inclusions hosted in the olivine and clinopyroxene of peridotites.
Chemical composition of amphibole and products of its alteration: BH-1G: 1 – kaersutite megacryst, 2–5 – products of kaersutite decomposition: 2 – rhonite, 3 – olivine, 4 – clinopyroxene, 5 – plagioclase. HP-205: 6 – kaersutite hosted in wehrlite. BH-19G: 7 – rhonite from clinopyroxenite. BH-20: 8 – pargasite xenocryst hosted in lherzolite. 9 – 11 – kaersutite and rhonite from host magmatites: 9 –kaersutite phenocrysts from basanites and nephelinites. HT: 10 – rhonite hosted in melt inclusions in olivine and clinopyroxene from lherzolites. 11 – rhonite from remnant glasses in nephelinites.
Chemical composition of plagioclase: HP-6: 1 – megacryst, core, 2 – megacryst, rim. SQR-012a: 3 – xenocryst, core, 4 – xenocryst, rim. 5 – plagioclase hosted in gabbro xenoliths. 6 – microlitic plagioclase in basanites.
Chemical composition of magnetite and spinel: A-6: 1 – magnetite megacryst, core, 2 – magnetite megacryst, rim; 3 – titanomagnetite phenocrysts hosted in magmatic rocks. BH-20: 4 – chrome spinel xenocryst. NH-536: 5 and 6 – chrome spinel xenocryst: 5 – core, 6 – rim. HA-21: 7 and 8 – hercynite megacryst: 7 – core, 8 – rim.
Chemical composition of apatite: HA-6: 1 – megacryst of fluorapatite. 2 – ultra-fluorine apatite hosted in basaltoids.

the outside, this aggregate is surrounded by a greenish-brown glass having isolated areas of saponite (Fig. 2b) and often zeolite. Judging by the composition of glass surrounding relict quartz, this was facilitated by the diffusion of magnesium and volatiles into the melting zone. Unlike the matrix pyroxene of the host rocks, fine-grained clinopyroxene formed on quartz is richer in SiO_2 and has a higher magnesium number (Mg* = 0.83–0.88); does not contain TiO_2 and Al_2O_3 (see Table 1). Quartz with a clinopyroxene rim is also found without glass formation, veined with calcite and buffered by it from the accreting microclinopyroxene aggregate.

Orthopyroxene. In the studied rocks, orthopyroxene is very unstable and is easily identifiable by the development of reaction kelyphite rims around it, represented by symplectic intergrowths of olivine and clinopyroxene (Fig. 3a) – products of the solid-phase decomposition of orthopyroxene peridotites, websterite and granulites. The width of rims comes up to 0.6 mm, with the structure being predominantly microequigranular, linearly elongated and with the long axes of decomposed minerals often arranged transversely to the boundary of the preserved orthopyroxene. In places, the olivine-clinopyroxene aggregate retains only small relicts of orthopyroxene (Fig. 3b), sometimes completely replacing it; in such cases, the aggregate acquires hypidiomorphic outlines (Fig. 3c). Some xenocrysts directly accrete newly formed augite or titanium augite from the host rocks (Fig. 3d). Complex bipyroxene inclusions (Fig. 3e), consisting of xenogenic ortho- and clinopyroxene (fragments of lherzolites or websterites) constitute noteworthy examples. In them, the orthopyroxene component has a symplectic olivine-clinopyroxene rim, with no changes occurring in the clinopyroxene part of the inclusions and both of these minerals accreting a newly-formed clinopyroxene. It is characteristic that bipyroxene xenocrysts also tend to develop a crystallographic form, which is typical of this group of minerals. The interstices of symplectic intergrowths are filled with feldspar, oligoclase, zeolite, saponite and calcite. Similar decomposition products of orthopyroxene are observed in the marginal zones of deep-seated xenoliths, including gabbros, where in places it is completely replaced by symplectite (Fig. 3f).

The petrochemical data (see Table 1) reveal two specific types of orthopyroxene xenocrysts: 1 – lherzolite having a high magnesium number (Mg* = 0.93–0.87), 2 – gabbro having a low magnesium number (Mg* = 0.70). According to this indicator, the composition of symplectic olivine and clinopyroxene is unstable and varies from 0.60 to 0.78 in peridotites, ranging from 0.57 to 0.76 in orthopyroxene gabbro, i.e. to up to values close to similar matrix minerals and the microphenocrysts of the host rocks. In the zone of orthopyroxene directly bordering the decomposition rim, its magnesium number decreases significantly, whereas the contents of Al_2O_3, CaO and sometimes K_2O increase (see Table 1).

Minerals compatible with host basic and ultrabasic alkaline rocks include olivine, clinopyroxene, amphibole, plagioclase, magnetite, spinel, apatite, nepheline and anorthoclase.

Olivine. The usual grain size comes to 0.3–0.8 mm, reaching 2–3 cm in megacrysts. The form varies from xenomorphic to idiomorphic. Corroded grains are often found with traces of pressure experienced before they were engulfed by ascending magma, fixed in the form of undulose extinction, which is unusual for the olivine (Fig. 4a). Some xenocrysts are decrystallised to one degree or another into a fine-grained mass having a microgranoblastic texture, with the size of individual grains ranging from 0.01 to 0.1 mm. Decrystallisation is mainly localised in grain margins, in places being developed in the form of spots or stripes (Fig. 4b), with smaller grains sometimes being decrystallised completely.

The chemical analysis of olivines (see Table 1) reveals that its central and marginal zones differ significantly in MgO and FeO contents, as well as in the magnesium number, 0.91–0.87 (depleted peridotites) and 0.82–0.83 (close to the magnesium number of olivine in the host rocks), respectively.

Clinopyroxene. The size of clinopyroxene is close to that of phenocrysts (0.6–0.8 mm); sometimes it forms megacrysts reaching up to 15 cm across. Its colour varies from colourless and slightly yellowish and brownish to brown-green, brownish-green and dirty green. As compared to orthopyroxene and olivine, it is more resistant to the influence of host rocks and is not accompanied by any noticeable phenomena of decomposition and decrystallisation. Nevertheless, a disturbance of its initial structure still occurs and is manifested by the formation of fractures and grains having a deconsolidated porous structure, which creates the effect of a non-specific shagreen surface. In the clinopyroxenes of large xenoliths, such structures are observed only in the areas where they are in contact with the host rocks and disappear in the inner parts, which indicates their occurrence under the influence of the host melt (Fig. 5a). Two types of mega- and xenocrysts of clinopyroxene are distinguished: 1 – ordinary; 2 – polygranular, i.e. intergrowths of several optically differently oriented grains combined into a pyroxene habit (see Figures 5c–f). Complex grains most often have a porous structure and accrete pure clinopyroxene from the host rocks. Grains having a green-grey (chromium diopside) porous central zone, as well as augite and titanium-augite non-porous marginal zones (see Fig. 5b) are also widespread, indicating the duality of the genesis of such formations. The pores are filled with minerals of most host rocks: feldspar, nepheline, titanaugite, zeolite, saponite, less often biotite, apatite and amphibole. In places, two-mineral olivine-clinopyroxene intergrowths occur, which are linked by a com-

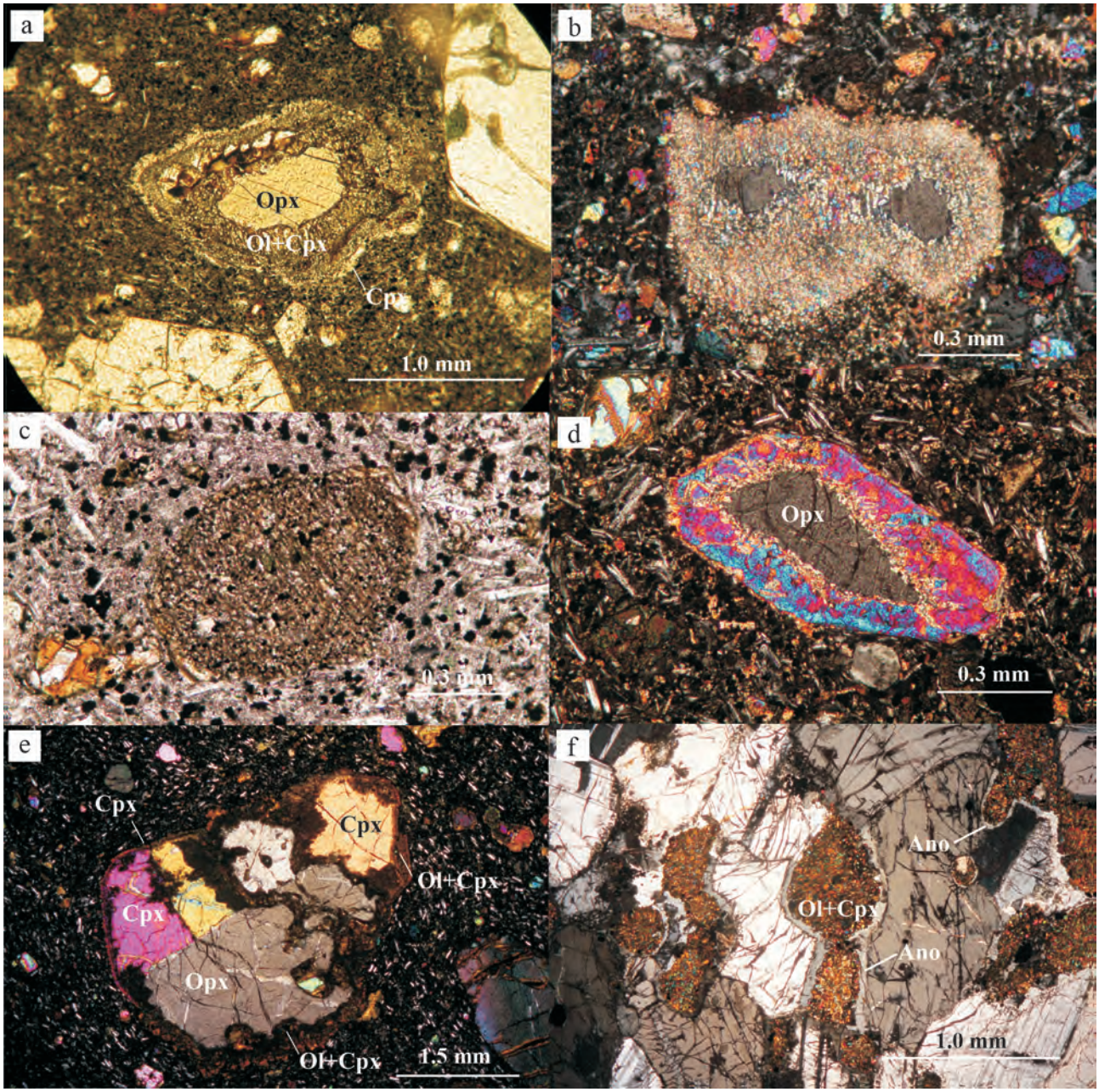

Fig. 3. Orthopyroxene xenocrysts and products of their alteration.

a – BH-107 (basanite): relic of *Opx* (greyish orange one in the centre) surrounded by the products of its decomposition: keliphitic rim composed of *Ol-Cpx* aggregate. The outer rim is composed of newly formed *Cpx* which growth was related to basanite crystallisation. PPL; b – HA-141 (basanite): almost complete pseudomorph of *Ol-Cpx* symplectite after *Opx* (two brownish grey relicts in the centre). XPL; c – SQR-45 (olivine basalt): *Opx* is completely replaced by *Ol-Cpx* symplectite and acquired subhedral pyroxene habit. PPL; d – CMR-622 (olivine basalt): bimodal xenocryst of pyroxene composed of *Opx*, brownish grey in the centre, overgrown by *Cpx* during the crystallisation of host melt. XPL; e – CMR-826 (olivine basalt): complex multigrain *Opx-Cpx* xenocryst (result of self-faceting) having a subhedral habit, in which *Opx* is recognised by *Ol-Cpx* symplectite with iddingsite after olivine. *Cpx* is recognised by a thin rim of *Cpx* overgrowth related to the crystallisation of host basalt. PPL and XPL, respectively; f – TH-53 (olivine basalt): xenolith of norite showing complete pseudomorphs of *Ol-Cpx* symplectite after orthopyroxene; symplectite is surrounded by thin anorthoclase (light grey) rims of metasomatic origin. XPL.

mon form characteristic of clinopyroxene, suggesting their kinship with peridotite xenoliths.

The chemical composition of clinopyroxenes (see Table 1) shows an increase in the concentrations of TiO_2, Al_2O_3 and FeO from the central to marginal zones of xenocrysts, with a decrease in SiO_2 and MgO in the opposite direction, including Mg*, which ranges from 0.90 to 0.87 (clinopyroxene peridotite) to 0.80

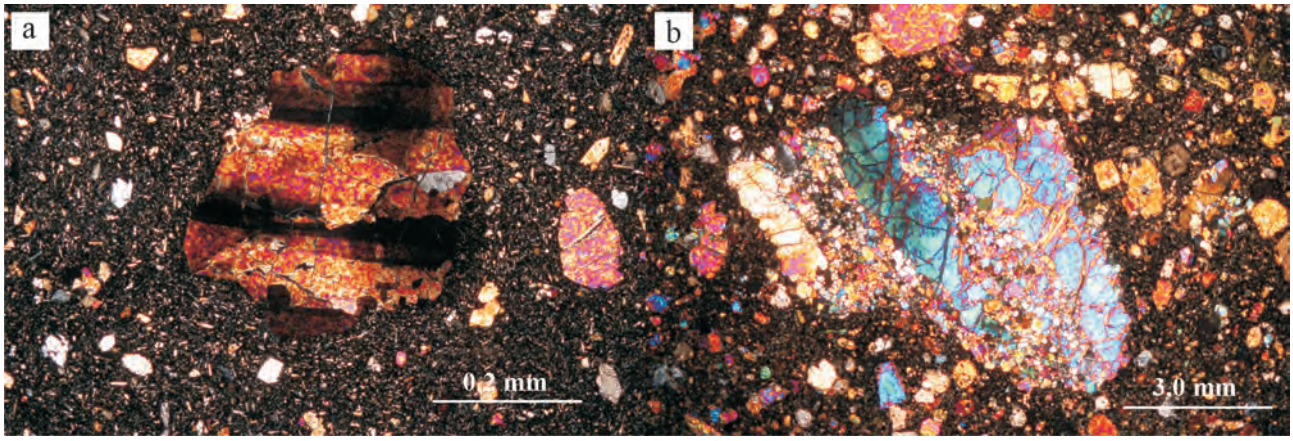

Fig. 4. Olivine xenocrysts.

a – HT-586 (basanite): remnant zebra-like texture of olivine xenocryst, that was acquired before the trapping of the grain by the host melt. XPL; b – NH-602 (nephelinite): Partly decrystallised megacryst of olivine; decrystallisation occurred according to pressurised textures. XPL.

(marginal zones of xenocrysts and phenocrysts of the host rocks). The internal parts of the xenocrysts are enriched with Cr_2O_3 (up to 0.95 wt %).

Amphibole is represented by kaersutite, whose size varies from that commensurate with phenocrysts to that of megacrysts (4.8 × 2.8 cm across). Its form is idiomorphic and hypidiomorphic. It is extremely unstable and is always characterised by a peculiar decomposition structure – polycrystalline symplectite, which forms partial or complete pseudomorphs after it with a large proportion of rhonite (Fig. 6a – c). In cases of incomplete pseudomorphs, kaersutite is usually located in their inner part. The same decomposition structures, both complete and incomplete, are developed in the xenoliths of peridotites and pyroxenites; however, they are xenomorphic and occupy intergranular spaces between olivine and pyroxene in them (Fig. 6d). In addition to rhonite, symplectite also includes titanium augite, olivine, plagioclase, titanomagnetite, zeolites and saponite. Individual xenocrysts are surrounded by a titanium augite rim. Along with titanomagnetite participating in the decomposition of amphibole, the marginal zone of symplectic pseudomorphs is enriched with the metasomatic titanomagnetite of the host basanites (Fig. 7). The structure of decomposition zones is eutectoid graphic.

The chemical composition of kaersutite and its decomposition products is shown in Table 1. Kaersutite differs from the primary pargasite of xenoliths in a lower magnesium number (0.71 and 0.80, respectively) and a higher content of TiO_2 (6.15 and 1.57 wt %, respectively), which is close to that of phenocrysts hosting magmatites. The magnesium number of rhonite (0.59–0.62) is lower than that of the rhonite from melt inclusions (0.73) and phenocrysts (0.75), with the magnesium number of rhonite from residual glasses and of late magmatic rhonite is even lower (0.48). All types of rhonite are characterised by a high content of TiO_2 (10.62–11.96 wt %). The olivine and clinopyroxene of symplectites are unequal in terms of the magnesium number (0.78 and 0.83, respectively). The composition of plagioclase in them varies from An_{53} to An_{62} (average An_{57}).

Plagioclase. The grain size comes up to 3.6 × × 2.0 cm, with the form varying from xenomorphic to hypidiomorphic. The central zones are represented by $An_{44\text{-}54}$, whereas plagioclase $An_{65\text{-}69}$ corresponding to the plagioclase of the host rocks is always developed along the margins. It is characterised by the development of crape structures and reactive interaction with the carrier magma, whose thermal effect is manifested by melting, less often decrystallisation. The initial stage of melting is manifested by the formation of a weakly birefringent porous zone (0.06–0.1 mm wide) having point inclusions of light brown, green or yellowish glass in the marginal zones of plagioclase or along the cracks in it (Fig. 8a). In the areas of more intense development of glass and simultaneously with it in plagioclase fingerprint-like structures are formed (Fig. 8b).

In the presence of calcite, the zones associated with the melting and development of such structures increase up to 0.2 mm. Xenocrysts, in which solid-phase decomposition of plagioclase into $An_{18\text{-}21}$ and $An_{60\text{-}62}$ takes place (Fig. 8c), are found more rarely. The most common type of changes is represented by the eutectoid symplectic intergrowths of plagioclase with titanium augite developing along its margins, along cracks and sometimes throughout the xenocryst area (Fig. 8d). In some places, the self-faceting of xenocrysts into prismatic forms that are characteristic of plagioclase is observed, which is also typical of the xenoliths of anorthosites (see Fig. 8b) recrystallised into megacrysts. Similar changes occur in the plagioclase of metagabbros.

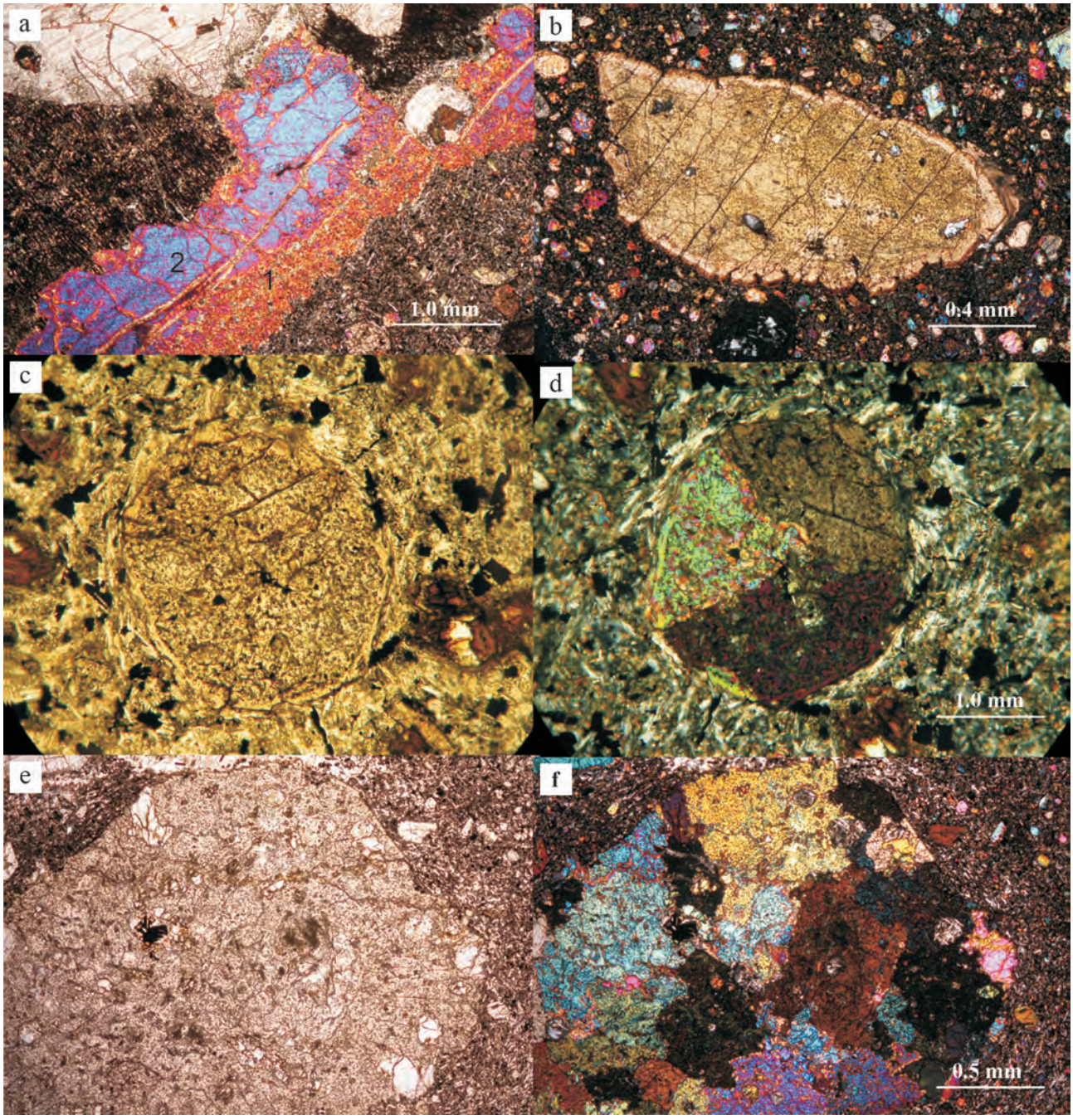

Fig. 5. Xenocrysts of clinopyroxene.

a – HP-385 (basanite): 1 – non-porous part of wehrlite xenolith remote from the contact with basanite; 2 – porous spongy zone of clinopyroxene at the contact with basanite is replaced by anhedral multi-mineral symplectite; the symplectite is of moderate brown colour and shows oriented texture with voluminous rhonite, XPL; b – (nephelinite): spongy xenocryst of fractured light brown chromian diopside overgrown by rims of newly-formed augite and titanium augite. XPL; c and d – BH-11 (basanite): the xenocryst of spongy clinopyroxene composed of three differently oriented grains with a thin rim of newly-formed augite; the augite rim shows sectorial extinction that is partly subordinated to the optical orientation of xenocryst segments. PPL and XPL, respectively; e and f – BH-815-17 (basanite): spongy multi-grained xenocryst of clinopyroxene from the xenolith of pyroxenite recrystallised into a subhedral habit. PPL and XPL, respectively.

The chemical composition (see Table 1) emphasizes the similarity of xenocrysts with the plagioclase of metagabbros, as well as their more basic peripheral rim with the plagioclase of the host basaltoids.

Anorthoclase. It is developed primarily in the form of megacrysts up to 3.5 × 2.8 cm in size. Sometimes anorthoclase preserves secondary muscovite (Fig. 9b), which clearly forms even before the xenocryst is en-

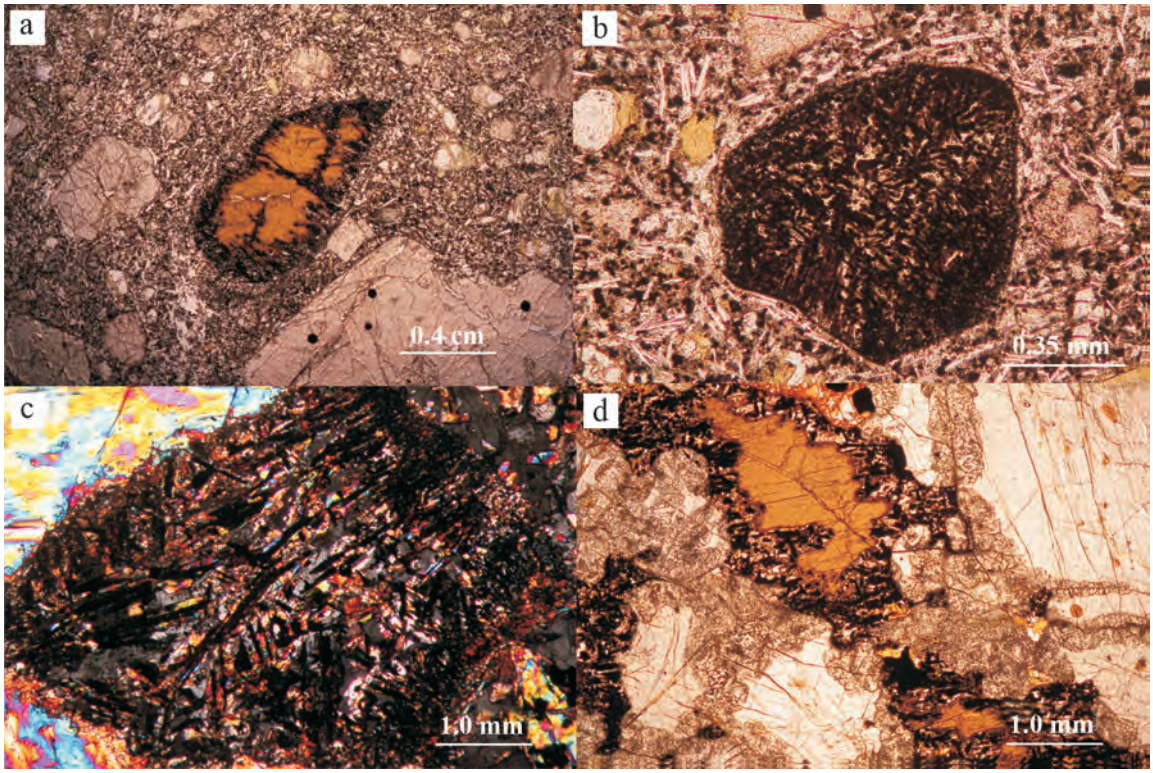

Fig. 6. Amphibole xenocrysts and products of their alteration.

a – CMR-734 (olivine basalt): a xenocryst of kaersutite with decomposition products composed of multi-mineral symplectite, which forms a keliphitic rim and fills the fractures; the xenocryst acquires a subhedral habit. PPL; b – HP-171 (olivine basalt): euhedral pseudomorphs of multi-mineral symplectite after amphibole; the symplectite is composed of voluminous rhonite (dark grey to greyish-black prismatic phase), titanium augite, olivine and plagioclase. PPL; c – BH-36 (basanite): complete pseudomorph of amphibole by multi-mineral symplectite, composed of rhonite (elongated brownish-grey to greyish-black prisms), plagioclase, clinopyroxene and olivine. XPL; d – CMR-749 (olivine basalt): anhedral kaersutite in the xenolith of clinopyroxenite is rimmed by a multi-mineral symplectite aggregate. PPL.

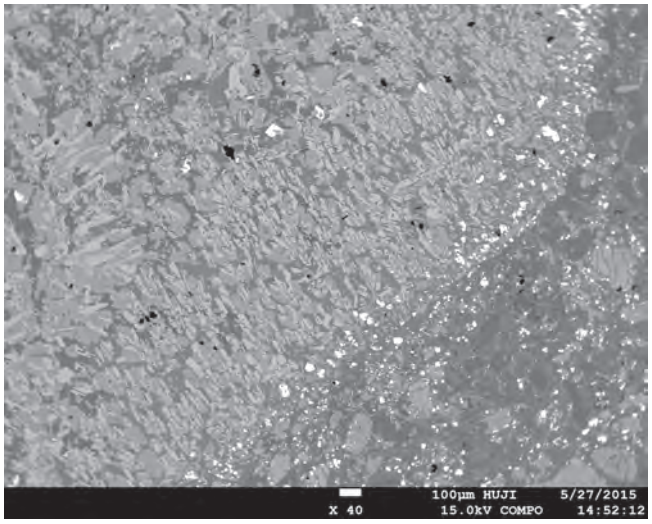

Fig. 7. BH-1G (basanite); BSE.

Complete pseudomorph of polycrystalline symplectite with voluminous rhonite after amphibole. Fine-grained inclusions of titanomagnetite, which formation was related to basanite crystallisation, are clearly seen in the endocontact zone of symplectite.

gulfed by the host rocks. In its marginal part, a melting zone (0.15 to 1.2 mm wide) is developed in places in the form of colourless and light brown or brownish glass, which at the border with relict anorthoclase is replaced by a zone of fingerprint-like structures (Fig. 9b). Sometimes changes are limited by the formation of such structures along the margins of a xenocryst (see Figures 9a and c), sometimes affecting the whole xenocryst. Xenocrysts are often veined with zeolite, calcite and, less commonly, saponite, as well as rimmed by them (1.2 mm wide zones). Similar changes with the formation of superimposed spherulitic and fingerprint-like structures occur to sodium-potassium feldspar also in the xenoliths of crystalloclastic tuffs of the Proterozoic crust (Fig. 9d).

The petrochemical characteristic of anorthoclase consists in the presence of quartz and hypersthene in the normative composition, which determines its formation from parent magma saturated with SiO_2, whereas normative nepheline is characteristic of anorthoclase from the host rocks (as an indicator of crystallisation from SiO_2-undersaturated melt). The composition of the glass resulting from the melting of anorthoclase

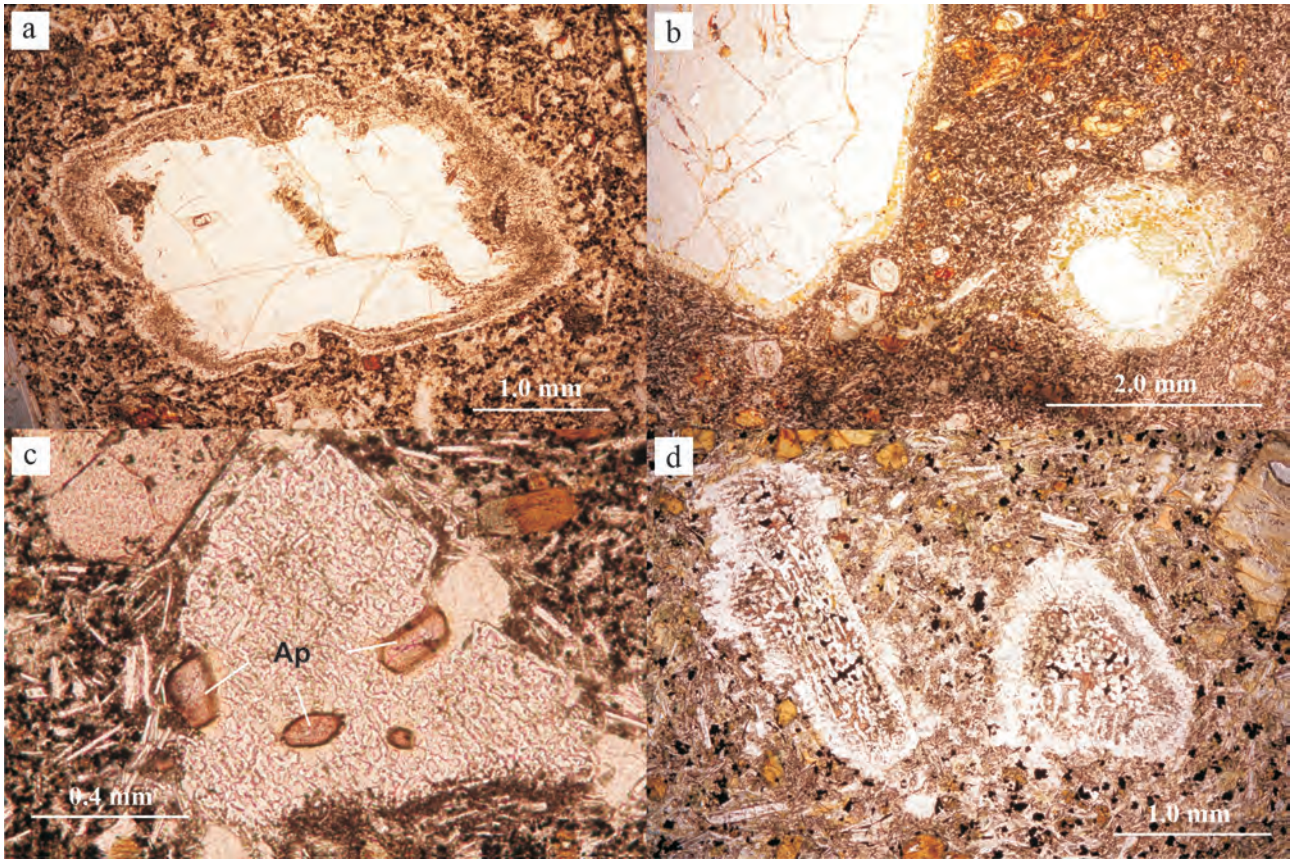

Fig. 8. Plagioclase xenocrysts.

a – SQR-30-1 (olivine basalt): a plagioclase xenocryst rimmed by a porous zone composed of newly-formed plagioclase; this is the initial stage of plagioclase alteration by the host melt. PPL; b – TH-43b (basanite): a fragment of anorthosite xenolith showing multi-grain xenocryst of plagioclase with the traces of partial melting in the border zone; the melting is revealed by the formation of pale yellowish-orange glass; the adjacent smaller xenocryst shows more extended rate of melting, with both pale yellowish-orange and dusky yellow spots of glass being observed. PPL; c – CMR-1096 (olivine basalt): a plagioclase xenocryst having a 'peresterite' texture of decomposition into albite-oligoclase and labradorite; the light brown inclusions in plagioclase are composed of fluorapatite of the host basanite. PPL; d – HP-197 (basanite): xenocrysts of plagioclase completely recrystallised into titanium augite-plagioclase symplectite displaying finger-print texture; the xenocrysts are rimmed by newly-formed plagioclase, whose content corresponds to host basanite. PPL.

reveals the addition of TiO_2, FeO, MgO, and volatiles, as well as the removal of Na_2O (Table 2).

Magnetite and spinel. Magnetite is found in the form of fragmented grains, with their size ranging from 0.3 mm to 2.0 cm. Reactive interaction with the host rocks is manifested by the development of a myrmekitic rim (0.03–0.22 mm wide) consisting of small inclusions of clinopyroxene, oligoclase and zeolite in its marginal zone (Fig. 10a). Myrmekitic rims clearly constitute deconsolidated near-contact zones, which the products of late crystallisation of basanites and nephelinites could permeate relatively easily.

Spinel is represented by two types: 1 – red-brown chromium spinel, 2 – grey-green and greenish-black hercynite spinel. The grains are clastic, with their size coming up to 1.0–1.3 mm. Usually, they have a titanomagnetite rim ranging from 0.04 to 0.2 mm in width (Fig. 10b, c). The formation of this rim is associated with the crystallisation of the bulk of the host rocks, including its late fluid phase represented by zeolite and saponite. Similar near-contact changes in spinel are also observed in peridotite xenoliths (Fig. 10d).

Geochemical data (see Table 1) show a significant increase in the content of TiO_2 in the marginal zones of magnetite and spinel up to the values close to those of titanomagnetite of the host rocks.

Apatite. It is found in the form of turbid grey fragmented grains up to 2.9 mm in size, in places with a well-developed plane-parallel texture, shear fractures and traces of decrystallisation, often covering their entire area (Figures 11a–c). It is veined with zeolite or saponite. The size of decrystallised apatite domains is from a micron to 0.13 mm. The same changes are observed in the xenoliths of apatite-magnetite and apatite-clinopyroxene-magnetite rocks (Fig. 11d). Decrystallisation constitutes an im-

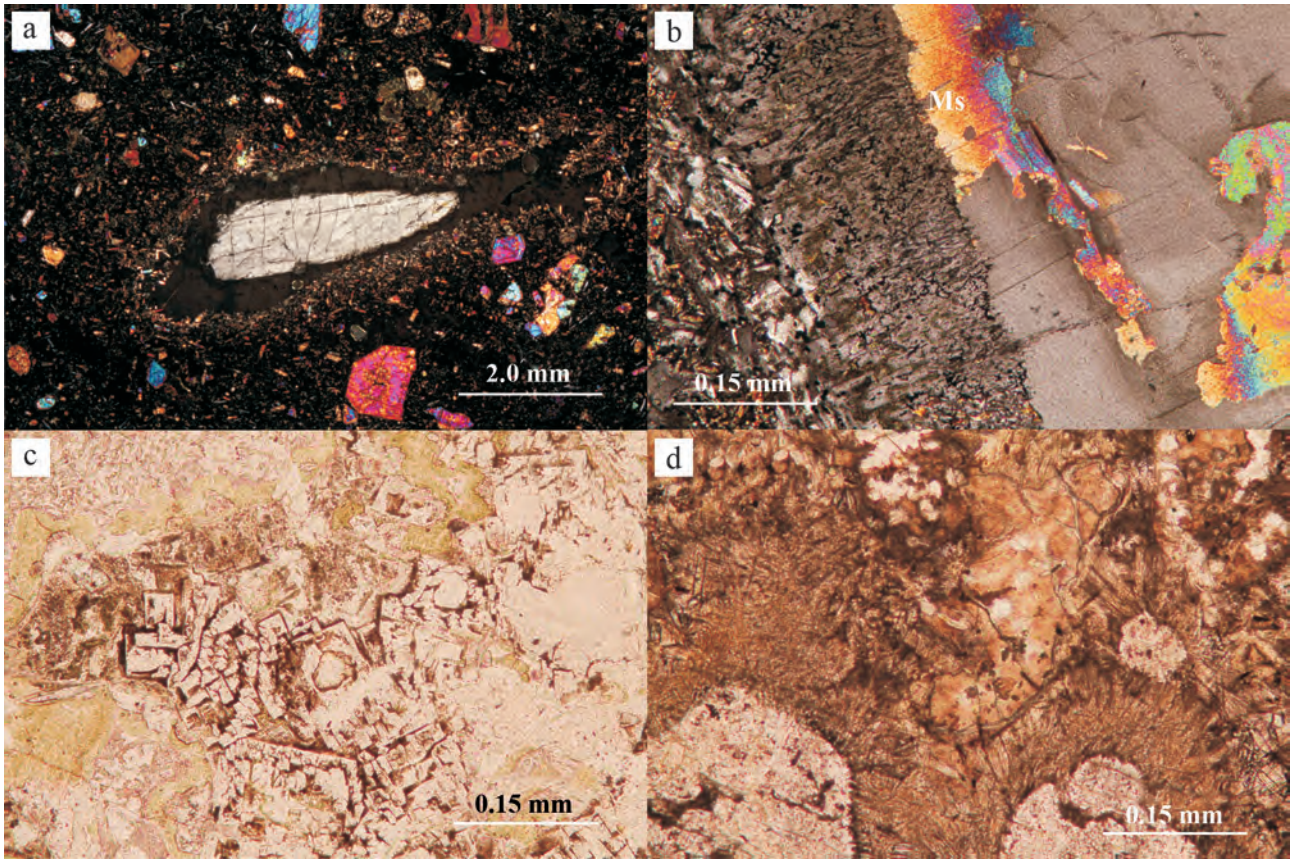

Fig. 9. Anorthoclase xenocrysts.

a – HG-2 (basanite). A xenocryst of anorthoclase rimmed by a melting zone. The glass phase is uncolored or of moderate brown colour. XPL; b – SQG-30-2 (olivine basalt). The rim of multi-grained anorthoclase xenocryst recrystallised into tiny domains with the formation of fingerprint-like texture and partial replacement of plagioclase by muscovite. XPL; c – HG-1907-3 (basanite). Completely recrystallised anorthoclase xenocryst with the fragment of fingerprint-like texture and moderate brown and pale olive glass. XPL; d – MG-2-2 (basanite). A xenolith of the upper crustal tuffs of the Zenifim Fm. Spherulitic texture develops around feldspars due to contact metamorphism induced by host basanite. PPL.

Table 2. Chemical composition of anorthoclase xenocrysts and products of their alteration, wt %

Element	1	2	3	4	5	Component	1	2	3	4	5
SiO_2	65.94	66.35	60.23	60.42	63.51	qu	3.51	4.80	16.58	29.13	–
TiO_2	0.15	0.01	0.33	0.41	0.38	or	23.22	20.45	24.76	21.69	25.23
Al_2O_3	20.79	20.40	18.93	18.97	21.17	ab	64.99	60.42	28.77	16.84	50.58
FeO	0.29	0.10	3.76	3.27	0.50	an	6.20	13.84	8.28	7.39	9.78
MnO	–	–	0.01	0.06	0.03	ne	–	–	–	–	4.39
MgO	–	–	0.91	–	0.15	c	1.65	0.05	5.77	9.01	–
CaO	1.24	1.06	1.67	1.49	2.38	hy	0.12	0.54	8.64	5.44	–
Na_2O	7.67	7.42	3.40	1.99	7.88	di	–	–	–	–	1.46
K_2O	3.92	5.40	4.19	3.67	4.27	wo	–	–	–	–	0.11
Total	100.00	100.74	93.43	91.18	100.27	il	0.30	0.06	0.63	0.78	0.72

Note. HG-3: 1 – megacryst. HG-2: 2 – megacryst, 3–4 – glass at the periphery of megacryst (product of its melting), 5 – anorthoclase from the matrix of host basanites.

portant difference between xenocrysts and the violet-blue microphenocrysts of fluorine-apatite host rocks. The apatite from xenocryst is also enriched with fluorine (see Table 1), most likely, under the influence of host magmatites.

Nepheline is much less common than other types of xeno- and megacrysts. It is found in the form of megacrysts reaching up to 4.0 × 2.0 cm in size, veined by zeolite, calcite and saponite, and often being surrounded by a continuous or interrupted rim of the same min-

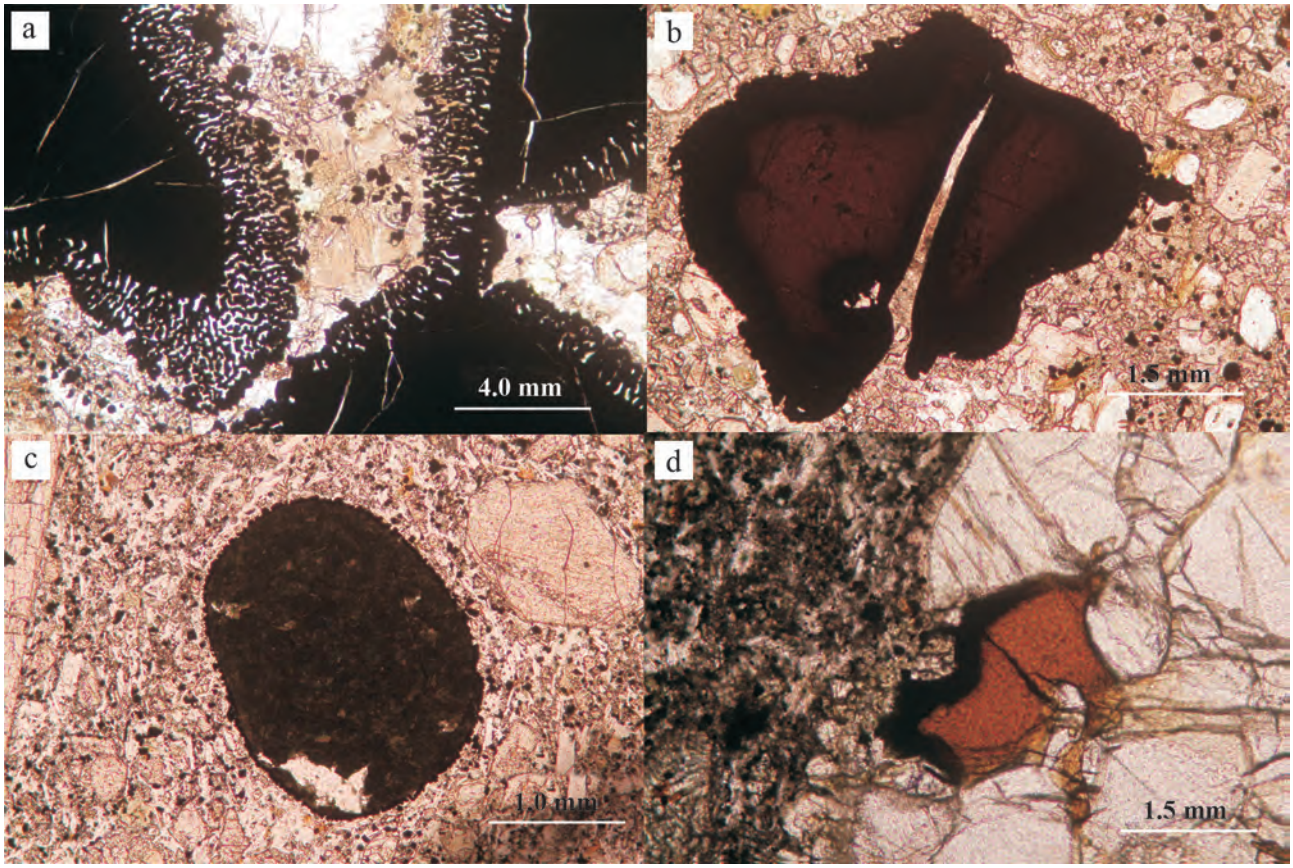

Fig. 10. Xenocryst of magnetite and spinel.

a – NH-254 (nephelinite). Myrmekite texture contouring the fragments of disintegrated magnetite megacryst. PPL; b – NH-369 (nephelinite). The xenocryst of chromian spinel showing a gradual transition into titanium magnetite. The veinlet of host melt contains zeolite at its end part and is completely surrounded by a rim enriched in titanium magnetite. PPL; c – TH-734 (basanite). A xenocryst of hercynite spinel with a thin rim of titanium magnetite, which formation occurred due to the crystallisation of host melt. PPL; d – HP-70 (olivine basalt). Chromian spinel in the xenoliths of lherzolite. The rim of titanium magnetite was formed only at the contact with host rocks. PPL.

erals (Fig. 12). No reactive changes were noted at the boundary of nepheline with the host rocks. For the rocks of PostArodcgl association, nepheline phenocrysts, which could be confused with xenocrysts, are generally not characteristic. In them, it is observed only as an interstitial mineral in the bulk of basanites and nephelinites.

RESULTS AND DISCUSSION

The presence of mantle and lower crustal high-density xenoliths along with the products of their disintegration (xeno- and megacrysts) in alkaline basalt and ultrabasic magmas of lower density and viscosity is due to their rapid rise to the earth's surface at a speed of 0.5–10 m/s [Ringwood, 1975; Kuo, Kirpatrick, 1985; Snelling, 2007]. A rapid rise causes decompression of xenoliths engulfed by magma, which were formed at a higher pressure, structural and polymorphic transformations of their constituent minerals, and ultimately leads to their melting. The lower limit determined by the thermodynamic conditions of these processes completely correlates with the results of studying melt and fluid inclusions in pyroxenes and olivines of the mantle xenoliths from Makhtesh Ramon, engulfed by the melt in the pressure range 5.9–8.1 kbar and temperatures of 1140–1350°C [Vapnik, 2005].

When magma is rising to the surface, xenoliths engulfed by it decompose into smaller fragments and individual minerals (xenocrysts) as a result of decompression. The latter are identified by similarities with xenolith minerals, in particular by deformity, characteristic sponginess ('clogging up'), reaction products, etc. Along with xenocrysts, the host rocks contain megacrysts that look like phenocrysts and often have a regular crystallographic form. There are different points of view on their genesis. Some researchers [Binns et al., 1970; Wilkinson, 1975; Evans, Nash, 1979; Ehrenberg, 1982; Irving, Frey, 1984; Dobosi et al., 2003; Kowabata et al., 2011] believe that the megacrysts of augite, spinel, anorthoclase, kaersutite, as well as other minerals, are formed during the crystallisation of host alka-

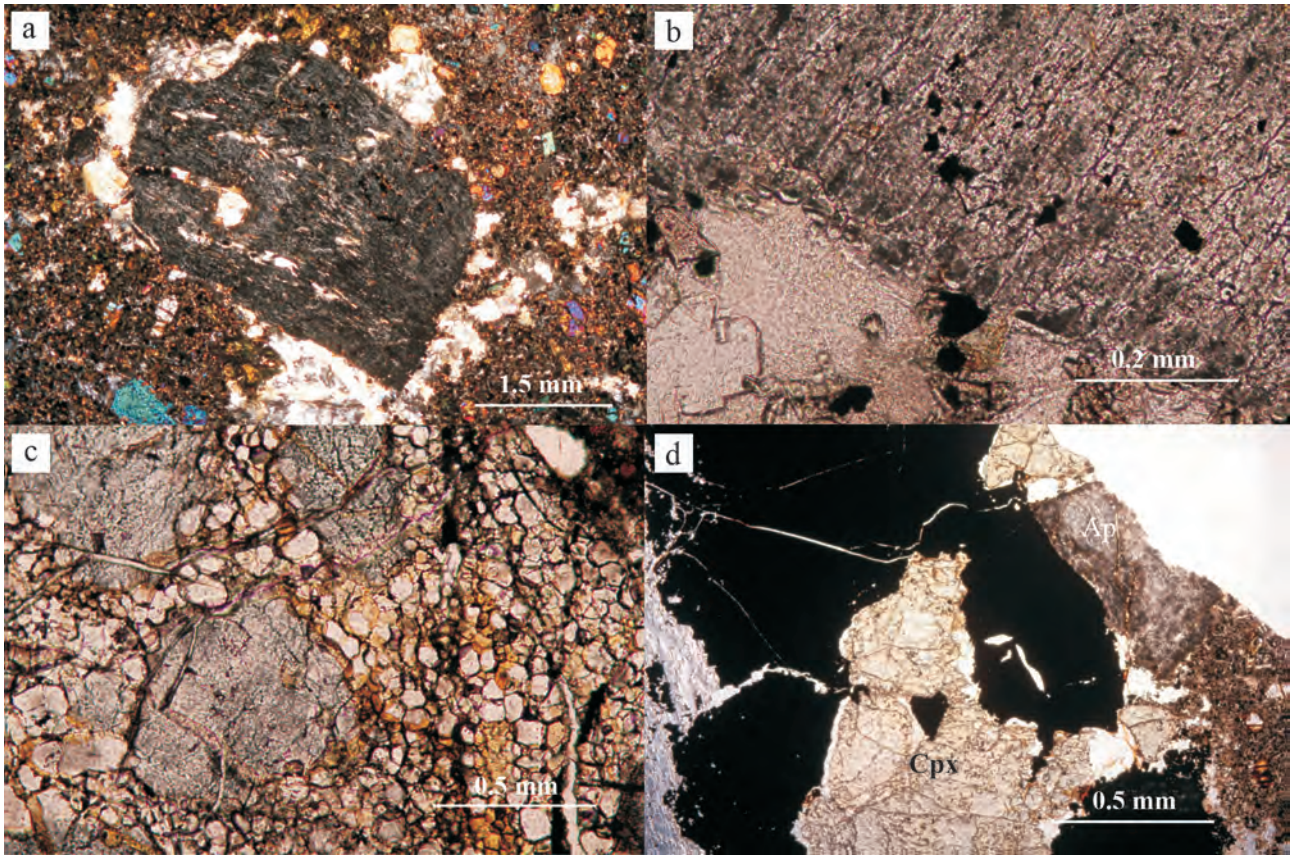

Fig. 11. Apatite xenocrysts.

a and b – HA-2 (basanite). A xenocryst of decrystallised apatite with fractures filled by zeolite. The enlargement shows the decomposition of apatite into numerous tiny domains. PPL; c – HA-6 (basanite) A fragment of partly decrystallised megacryst of apatite. PPL; d – HA-12 (basanite). A xenolith of apatite-clinopyroxene-magnetite rock. The moderate brown grain of decrystallised apatite is on the right side. PPL.

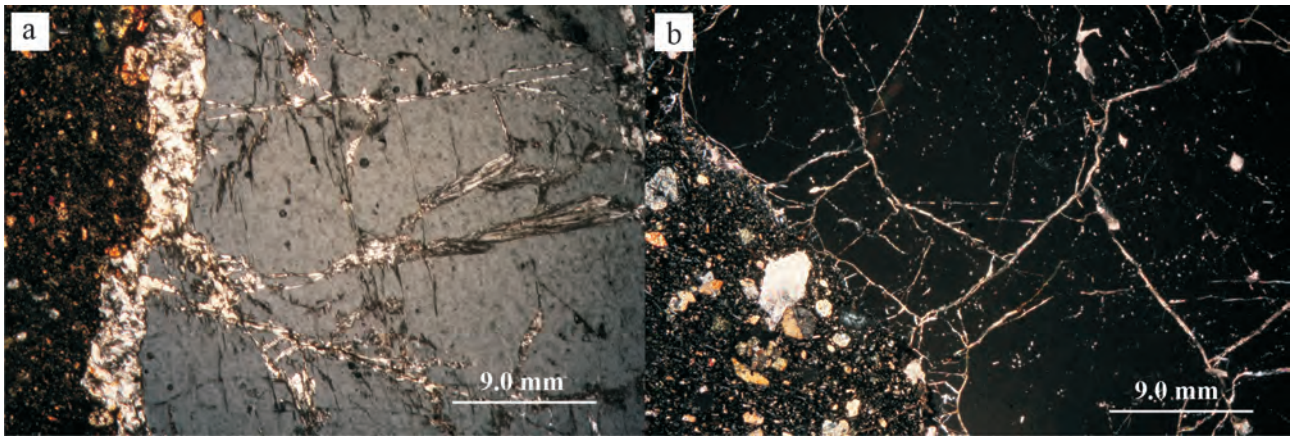

Fig. 12. Nepheline xenocrysts.

a – HG-2035 (nephelinite). A fractured xenocryst of nepheline, with the outer rim and veinlets being composed of zeolite. The genesis of zeolite is related to the crystallisation of host nephelinite. XPL; b – HG-2013 (basanite). Analogous to the previous sample, but the veinlets are composed of calcite. XPL.

line-basaltic magmas and constitute products of deep-seated intermediate foci or fragments of previous metasomatites. However, others [Shulze, 1987; Righter, Carmichael, 1993; Barns, Roeder, 2001; Rankenburg

et al., 2004] call them xeno-megacrysts – fragments of peridotites, gabbros, pyroxenites and syenites – due to the inconsistency with the conditions for the formation of host magmas. In [Nielson, Nakata, 1994; Shaw, Eyzaguirre, 2000], the key emphasis is placed on the heterogeneity of megacrysts: some of them are rejected by the metasomatic mantle, others constitute cumulates of the host magmas.

The effect of the host melt on the solid phases engulfed by it is characterised by a wide range of transformations of the latter: changes in petrographic and chemical features, solid-phase decomposition reactions, decrystallisation and recrystallisation. Being separated from xenoliths, individual constituent minerals are surrounded by melt and, as a result, experience an even more significant temperature shock, which generally corresponds to pyrometamorphism, leading to melting.

Melting

Xenocrysts displaying clear signs of melting include quartz and feldspar. Quartz is primarily engulfed by magma from the Mesozoic formations in the area, partially from Proterozoic tuffs and quartz-bearing granulites, which indicates that interaction between quartz and the host melt takes place at a relatively small depth. The melting point of quartz (1723–1728°C) is 350–400°C higher than the temperature at which melt inclusions in the minerals of xenoliths from Makhtesh Ramon are engulfed [Vapnik, 2005]. Nevertheless, its melting is an obvious fact and clearly occurred at a lower temperature. According to [Ostrovskii et al., 1959; Kennedy et al., 1962], the melting of quartz with its preliminary transition to tridymite and cristobalite under the conditions of crustal pressure can occur in the temperature range of 1200–1300°C, i.e. under conditions that are completely consistent with the engulfment of the aforementioned melt inclusions.

The melting of plagioclase begins with the formation of a turbid grey deconsolidated rim along its margins with a small amount of glass and the development of lattice and fingerprint-like structures (with interstitial glass between plagioclase domains). As shown by the experiments of [Tsuchiyama, 1985, 1986; Nelson, Montana, 1992], plagioclase easily undergoes such transformations at low pressure and high temperature (1190–1307°C), i.e. under thermodynamic conditions that are quite applicable to the interaction between xenocrysts and alkaline basaltoids in Makhtesh Ramon.

The megacrysts of anorthoclase are subject to more intense melting than quartz and plagioclase. At the boundary with the host melt, it melts to form glass or spherulite, followed by a zone of lattice and fingerprint-like structures. The emergence of a spherulitic structure, as suggested by [Arzill, Carroll, 2013], indicates the extreme heating of the mineral under crustal pressure, which is confirmed by the corresponding transformations in the potassium feldspar of xenoliths from Proterozoic tuffs.

Solid-phase decomposition

The processes of solid-phase decomposition, represented by symplectites, are characteristic of the xenocrysts of orthopyroxene, amphibole, sometimes plagioclase; they are manifested in the form of kelyphite rims, linear zones and complete pseudomorphs.

Orthopyroxene decomposes into a microlite aggregate of olivine and clinopyroxene. This phenomenon is extensively covered in the literature [Kutolin et al., 1976; Agafonov et al., 1978; Messiga, Bettini, 1990; Arai, Abe, 1995; Kogarko et al., 2001; Villaseca et al., 2010] and reproduced in experimental studies [Boivin, 1980; Brearley, Scarfe, 1986; Shaw et al., 1998]. A feature distinguishing the described decomposition structure from the one observed by the indicated authors is the absence of glass in it, which in the intergranular spaces is replaced with feldspars, as well as zeolite and saponite rich in the hydroxyl component.

Symplectites after kaersutite are composed of rhonite, titanium-augite, olivine, plagioclase, titanomagnetite and late magmatic minerals. Rhonite is an indicator of the thermodynamic conditions for the solid-phase decomposition of amphibole and, according to [Kyle, Price, 1975; Johnston, Stout, 1984; Vapnik, 2005; Lopez et al., 2006; Grapes, Keller, 2010; Sharygin et al., 2011], is stable in the temperature range 1000–1260°C and pressures of 0.5–4.0 kbar. The experimental studies of orthopyroxene [Brearley, Scarfe, 1986; Shaw, 1999; Kogarko et al., 2001; Miller et al., 2012] and amphibole [Ban et al., 2004] show that their decomposition results in the formation of glass rich in SiO_2. In the studied samples, such glass was not found. The presence of minerals such as zeolite, saponite, and calcite in the interstitial of decomposition products indicates the importance of the fluid component of the magmatic melt in this process. The likelihood of such reactions involving the rapid crystallisation of the melt into a fine crystalline mass (without glass formation) is also experimentally justified [Chepurov et al., 2013].

Another form of solid-phase decomposition is occasionally observed in plagioclase xenocrysts and is manifested by the formation of a peristerite structure in them, which differs from the ordinary peristerites of metamorphic rocks in the higher compositions of coexisting plagioclases – $An_{18\text{-}21}$ and $An_{60\text{-}62}$. The probability of such a structure in main plagioclases was experimentally reproduced in [Ribbe, 1960] and was suggested in [Miyashiro, 1976].

Decrystallisation and recrystallisation

Decrystallisation (thermal destruction) as a sign indicating the difference between xenocrysts and phenocrysts is most clearly manifested in olivine and ap-

atite, less often in plagioclase. It develops by forming areas in xenocrysts, which have a micrograin structure and are confined to marginal or weakened (linear) zones. The combination of the newly formed structure with pressurised structures ('zebra-like' in olivine, plane-parallel in apatite, bent in plagioclase) within a single grain suggests that decrystallisation is a reaction to the removal of residual stress in these minerals under new decompression conditions. In addition, it exhibits a tendency for the equalization of the composition of restructured xenocrysts and the eponymous minerals of the host rock matrix.

Recrystallisation (thermal reconstruction) constitutes one of the most important processes characterising the structural rearrangement of xenocrysts under the influence of the surrounding high-temperature melt. Almost all minerals of xenocrysts, both mono- and polygranular, underwent structural rearrangement. They share the ability to transform initially xenomorphic grains (before the disintegration of xenoliths) into crystallographically regular forms similar to the phenocrysts of the host rocks. By analogy with the processes considered in biology and biophysics, this phenomenon of morphological rearrangement is called structural homeostasis [Goryainov, Ivanyuk, 2010]. Particularly interesting in this respect are multi-grain intergrowths, which in fact are small xenoliths of clinopyroxenites, olivinites and plagioclasites characterised by a granoblast structure, illustrating a clear tendency to reacquire their genetically characteristic form, clearly observed in clinopyroxenes and olivines. Transformation is also characteristic of initially xenomorphic (in xenoliths) kaersutite, of its varieties completely transformed into symplectites, as well as of complete symplectites after orthopyroxene. Other minerals are sometimes used, including minerals similar to them in chemistry, for example, olivine and orthopyroxene in clinopyroxene in order to build a perfect habit. In the course of self-faceting, a certain sequence can be established: the crystallographic rearrangement of the granoblast aggregate within the framework of a common perfect habit – the emergence of the initial signs of twinning and zoning – optical homogenisation, i.e. the transformation of variously oriented grains into a normal crystal. The ability of crystals to restore the forms of natural faceting under the conditions of free growth, along with their self-organisation, has long been known and has been described as the 'method for the crystallisation of balls' by Artemyev [Shubnikov, 1935] and 'the spontaneous crystallisation by Lukirsky' [Geguzin, 1987] and is explained by the tendency of the mineral to provide the least surface energy.

GEOCHEMICAL TRANSFORMATIONS

When interacting with the carrier melt, all ontogenetic changes occurring in xenocrysts are directed at the geochemical equalisation of their compositions with minerals crystallising from this melt and are manifested by the diffuse and infiltration substitution of xenocrysts with the chemical elements of the surrounding melt. Diffuse substitution is most noticeable in the marginal zones of xenocrysts and is manifested by the emergence of marginal zones in them, which completely correspond to the minerals of the host rocks in terms of composition. Thus, the xenocrysts of clinopyroxene, orthopyroxene and amphibole accrete augite and titanium augite, with plagioclase acquiring a high-anorthite rim, whereas spinel and magnetite get a titanomagnetite rim. Bimodal crystals, in which the xenocryst is a seed component inducing the development of a later phase associated with crystallisation of the host melt, are obtained.

On the whole, the geochemical data reveal a tendency for the xenocrysts of pyroxene and olivine to decrease magnesium contents, increase the concentrations of iron contents, and, accordingly, decrease the magnesium number to those of the host minerals rocks in the direction from the centre to the marginal zone.

Statistical geochemical data on the distribution of SiO_2 (wt %), magnesium number and anorthite number in xenoliths, xenocrysts and eponymous minerals of host magmatites are of interest. The histograms (Figures 13 and 14) and the diagram (Fig. 15) reflect the distribution of SiO_2 values (wt %) and the magnesium number in the olivines and clinopyroxenes of xenoliths, xenocrysts and host magmatites. In constructing them, data from previous studies were used, in which all inclusions in the rocks of the studied association were phenocrysts and, therefore, were identified as a group of phenocrysts without being divided into phenocrysts and xenocrysts. As Figures 14 and 15 show, the magnesium number in the olivines and clinopyroxenes of xenocrysts and xenoliths reveal a tendency towards the equalisation with the eponymous minerals of the host rocks. Mg* = 0.85–0.87 should be considered the boundary value, the limiting value for the olivine and clinopyroxene of melt inclusions in the minerals of xenoliths of peridotites, matrix grains and microphenocrysts of the host rocks. Higher values apply to xenoliths and xenocrysts. The distribution of SiO_2 (see Fig. 13) in clinopyroxenes and olivines also follows this trend and, at the same time, illustrates that the increased primary contents of this element are well correlated with increased magnesium numbers (see Fig. 15) in xenoliths and xenocrysts, which distinguishes them from phenocrysts. In terms of silica content, the dividing line is at 40.0 wt % for olivines and 50.0 wt % for clinopyroxenes: higher contents are characteristic of xenoliths and xenocrysts, with lower contents being typical of host rocks, thus emphasising their belonging to the geochemical type of silica-saturated and undersaturated rocks, respectively. The presence of the undivided inclusions of olivine and clinopyroxene characterised by high SiO_2 and magnesium numbers in the samples of the magmatic rock group that exceed the boundary sta-

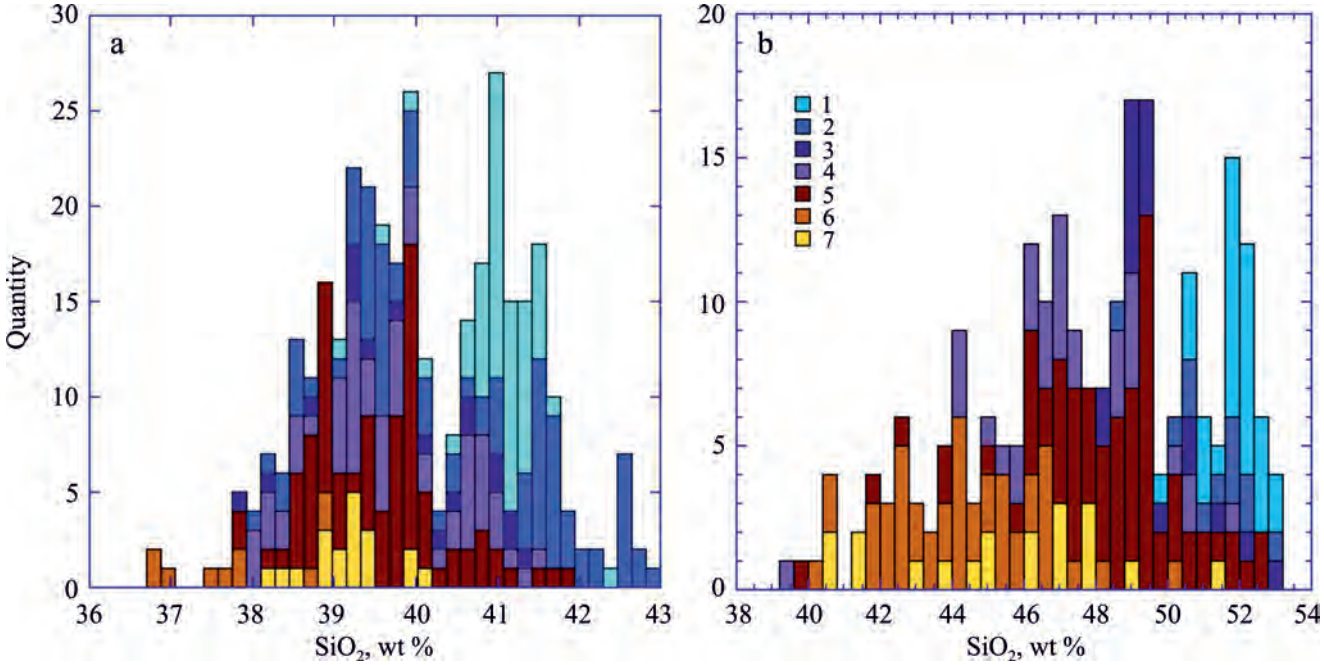

Fig. 13. SiO_2 content in olivine (a) and clinopyroxene (b) hosted in xenoliths (including xenocrysts) and magmatic rocks.

Xenoliths: 1 – harzburgites, 2 – lherzolites, 3 – wehrlites, 4 – clinopyroxenites and websterites; magmatic rocks: 5 – all mineral inclusions without being subdivided into phenocrysts and xenocrysts, 6 – mineral inclusions in matrix and prismatic microphenocrysts from host magmatic rocks, 7 – mineral phases in melt inclusions hosted in the olivine and clinopyroxene of peridotite xenoliths.

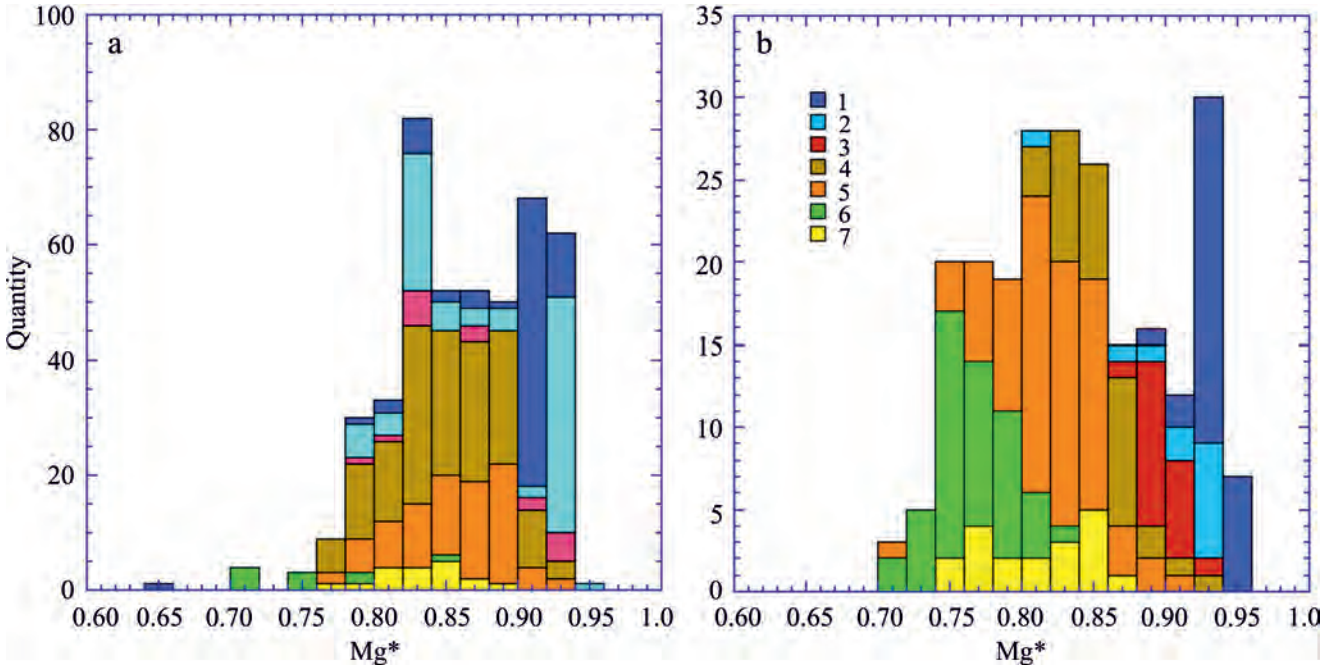

Fig. 14. Mg* distribution in olivine (a) and clinopyroxene (b) hosted in xenoliths (including xenocrysts) and magmatic rocks.

Xenoliths: 1 – harzburgites, 2 – lherzolites, 3 – wehrlites, 4 – clinopyroxenites and websterites; magmatic rocks: 5 – all mineral inclusions without being subdivided into phenocrysts and xenocrysts, 6 – mineral inclusions in matrix and prismatic microphenocrysts from host magmatic rocks, 7 – mineral phases in melt inclusions hosted in the olivine and clinopyroxene of peridotite xenoliths.

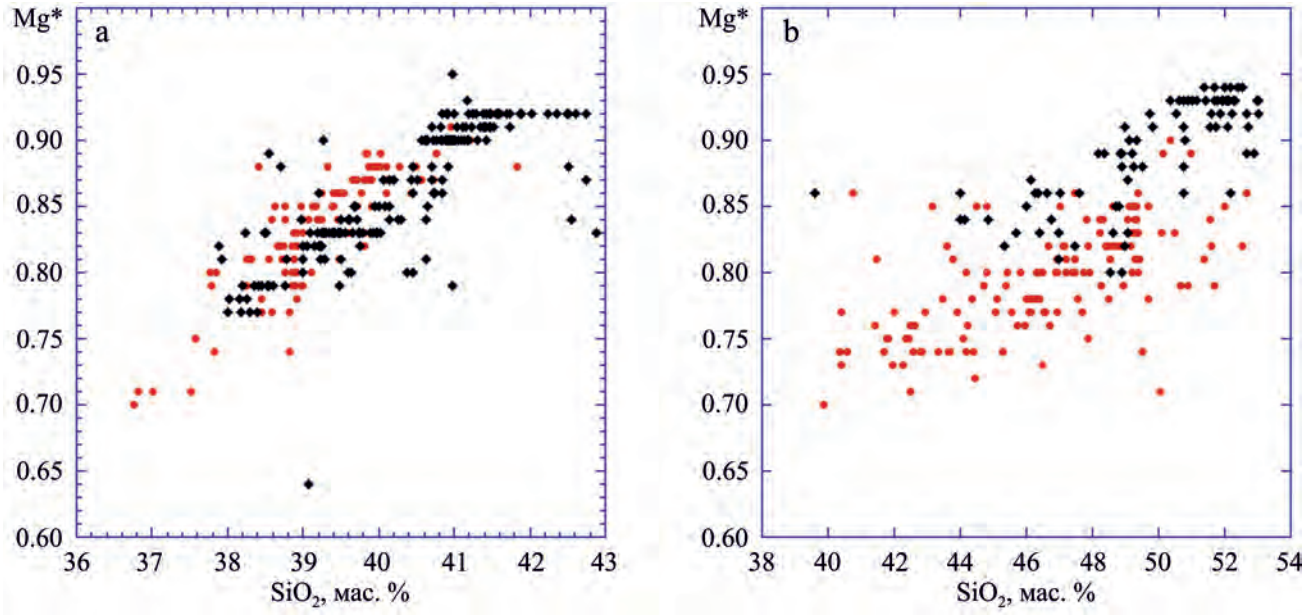

Fig. 15. Correlation between SiO_2 and Mg* in olivine (a) and clinopyroxene (b) hosted in xenoliths (including xenocrysts) and magmatic rocks.

Black rhombi denote combined sample of harzburgites, lherzolites, wehrlites, clinopyroxenites and websterites; red circles denote combined sample of all magmatic rocks.

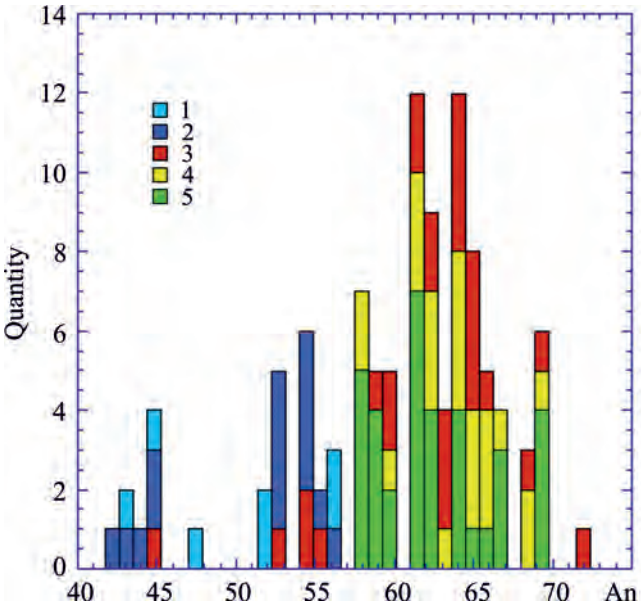

Fig. 16. Anorthite distribution in plagioclase hosted in metagabbro xenoliths (granulites), xenocrysts, and magmatic rocks.

1 – metagabbro, 2 – xenocrysts, 3 – mineral inclusions in host olivine basalts and basanites (all mineral inclusions without being subdivided into phenocrysts and xenocrysts), 4 – prismatic microphenocrysts, 5 – microliths.

tistical values indicates the presence of xenocrysts in these samples. If we consider the distribution of the An-component in the plagioclases of xenocrysts, metagabbros and host rocks (Fig. 16), we can see that the interface between them and the plagioclase of the host rocks runs at $An_{57–58}$: lower values (from An_{42} to An_{57}) are characteristic of xenocrysts and xenoliths, whereas higher values (from An_{57} to An_{73}) are typical of host basaltoids. At the same time, the group of undivided inclusions reveals values characteristic of plagioclase xenocrysts.

Infiltration metasomatism covers almost all xenocrysts to one degree or another, given that decompression disarranges the structure of crystals, leads to their deconsolidation and the formation of fractures that facilitate the percolation of the host magma and its fluids through them. This is especially noticeable in the xenocrysts of clinopyroxene, in which traces of percolation are marked by the so-called spongy structures, manifested by a non-specific shagreen texture. The formation of such structures constitutes a complex issue and has been considered in a number of works. Some researchers believe that partial melting of the mantle triggers the infiltration of gas-water fluids [Dal Negro et al., 1989; Francis, 1991; Carpenter et al., 2002], whereas others explain it by the interaction of xenoliths with magmatic fluids when rising to the surface under the conditions of rapid pressure reduction [Kutolin et al., 1976; Agafonov et al., 1978; Tsuchiyama, 1986; Wang et al., 2012], which completely consistent with our data.

The peculiar symplectites of plagioclase, represented by its eutectoid intergrowths with titanium augite, also belong to the products of infiltration substitution.

The plagioclase in them has a lattice and fingerprint-like structure, the same as in the zones of initial melting of this mineral. However, due to the diffusion of FeO, MgO, and TiO_2 from the surrounding melt titanium augite is formed in it. A similar situation involving the enrichment of symplectic pseudomorph after kaersutite with titanomagnetite at the boundary with the host basalt is shown in Fig. 7. The same type of metasomatism should include the formation of myrmekite texture in the marginal zone of magnetite xenocrysts, which bears only an external resemblance to the real myrmekite texture of solid-phase decomposition and is caused by the penetration of minerals in the final stage of crystallisation of the host melt into its deconsolidated margins.

CONCLUSION

The study shows the important role of ordinary microscopic observations, which provide the opportunity to detect clear signs of differences between genetically heterogeneous formations – phenocrysts and xenocrysts – coexisting in a single magmatic system. Some xenocrysts, in particular, quartz and orthopyroxene, which are incoherent with respect to the alkaline-basaltoid and nephelinite melts hosting them, are identified easily, whereas the identification of other minerals (in particular olivine, clinopyroxene, amphibole, plagioclase, anorthoclase, nepheline, magnetite and apatite) nominally corresponding to the possible crystalline phases of the melts, is often difficult. Nevertheless, the use of a number of informative petrographic and geochemical features makes it quite possible. The main factors that trigger mechanisms underlying the interaction between the melt and xenoliths are decompression, high-temperature metamorphism and metasomatism. Decompression leads to the disintegration of xenoliths into smaller fragments and individual minerals, the destruction, as well as deconsolidation, of these minerals, the formation of pores, caverns and channels, activating the percolation of fluids dissolved in the melts. Metamorphism corresponds to the highest temperature facies of contact metamorphism; for a number of minerals, it results in partial melting, while metasomatism developing in this context is directed at equalising the compositions of xenocrysts and crystallisation products of the melt hosting them.

The most important criteria contributing to the identification of xenocrysts include partial melting, solid-phase decomposition, decrystallisation of initial structures (before-trapping), recrystallisation (self-faceting) of initially xenomorphic grains into crystallographically more perfect forms, as well as a change in composition due to the metasomatic effect of the host magma.

REFERENCES

Agafonov L.V., Kutolin V.A., Lesnov F.P. (1978) Influence of basaltic magma on xenoliths of ultramafic and mafic rocks, and relative stability of minerals in basaltic melt. *Materialy po petrologii i mineralogii ultraosnovnykh i osnovnykh porod* [Materials on petrology and mineralogy of ultamafic and mafic rocks]. Novosibirsk, Nauka Publ., 67-84. (In Russian)

Arai S., Abe N. (1995) Reaction of orthopyroxene in peridotite xenoliths with alkali basalt melt and its implication for genesis of alpine-type chromitite. *Amer. Mineral.*, **80**, 1041-1047.

Arzilli F., Carroll M.R. (2013) Crystallization kinetic of alkali feldspars in cooling and decompression induced crystallization experiments in trachytic melt. *Contrib. Mineral. Petrol*., **166**, 1011-1027.

Baer G., Heimann A., Eshet Y., Weinberger R., Musset A., Sherwood G. (1995) The Saharonim Basalt: A Late Triassic – Early Jurassic intrusion in south-eastern Makhtesh Ramon. *Isr. J Earth Sci*., **44**, 1-10.

Ban M., Witt-Eickschen G., Klein M., Seck H. (2004) The origin of glasses in hydrous mantle xenoliths from the West Eifel, Germany: incongruent break down of amphibole. *Contrib. Mineral. Petrol*., **148**, 511-523.

Barns S., Roeder P. (2001)The range of spinel composition in Terrestrial mafic and ultramafic rocks. *J. Petrol*., **42**, 2279-2302.

Bédard J.H. (1988) Comparative amphibole chemistry of the Monteregian and White Mountain alkaline suits, and the origin of amphibole megacrysts in alkali basalts and lamprophyres. *Miner. Mag*., **52**, 91-103.

Bentor Y. (1952) Magmatic intrusion and lava sheets in the Raman area of the Negev (southern Israel). *Geol. Mag*., **89**, 129-140.

Binns R., Duggan M., Wilkinson J. (1970) High pressure-megacryst in alkaline lavas from northeastern South Wales with chemical analyses. *Amer. J. Sci*., **269**, 132-168.

Boivin P. (1980) Données expérimental préliminaries sur la stabilité de la rhönite à 1 atmosphère. Application aux gisements naturels. *Bull. Minéral*., **103**, 491-502.

Bonen D., Perlman I., Yelin J. (1980) The evolution of trace element concentrations in basic rocks from Israel and their petrogenesis. *Contrib. Mineral. Petrol*., **72**, 397-414.

Brearley M., Scarfe C.M. (1986) Dissolution rates of upper mantle minerals in alkali basalt melt at high pessure: an experimental study and implications for ultramafic xenoliths survival. *J. Petrol*., **27**, 1157-1182.

Carpenter R., Edgar A., Thibault Y. (2002) Origin of spongy textures in clinopyroxenes and spinel from mantle xenoliths, Hessian Depression, Germany. *Mineral. Petrol*., **74**, 149-162.

Chepurov A.I., Zhimulev E.I., Agafonov L.V., Sonin V.M., Chepurov A.A., Tomilenko A.A. (2013) The stability of ortho- and clinopyroxenes, olivine, and garnet in kimberlitic magma. *Geol. Geofiz*., **54**(4), 533-544. (In Russian)

Dal Negro A., Manoli S., Secco L., Piccirillo E.M. (1989) Megacrysticclinopyroxenes from Victoria (Australia): crystal chemical comparisons of pyroxenes from high and low pressure regimes. *Eur. J. Mineral*., **1**, 105-121.

Dobosi G., Downes H., Emdey-Istin A., Jenner J. (2003) Origin of megacrysts and pyroxenite xenoliths from the Pliocene alkali basalts of the Pannonian basin (Hungary). *J. Mineral. Geochem.*, **178**, 217-237.

Ehrenberg S. (1982) Petrogenesis of garnet lherzolite and megacrystalline nodules from the Thumb, Navajo volcanic field. *J. Petrol*., **23**, 507-547.

Evans S., Nash W. (1979) Petrogenesis of xenoliths-bearing basalts from southeastern Arizona. *Amer. Mineral*., **64**, 249-267.

Eyal M., Becker A., Samoilov V. (1996) Mt. Arod – an Early Cretaceous basanitic volcano with a fossil lava lake. *Israel J. Earth Sci*., **45**, 31-38.

Fershtater G., Yudalevich Z. (2017) Mantle metasomatism and magma formation in continental lithosphere: data on xenoliths in alkali basalts from Makhtesh Ramon, Negev desert, Israel. *Petrology*, **25**, 181-205.

Fershtater G.B., Yudalevich Z.A., Khiller V.V. (2016) Xenoliths in alkaline basaltoids of Makhtesh Ramon (Negev, Israel) as indicators of mantle metasomatism and magma genesis. *Litosfera*, (3), 5-26. (In Russian)

Francis D. (1991) Some implications of xenoliths glasses for the mantle sources of alkaline mafic magmas. *Contrib. Mineral. Petrol*., **108**, 175-180.

Garfunkel Z., Katz A. (1967) New magmatic features in Makhtesh Ramon, southern Israel. *Geol. Mag*., **104**, 608-629.

GeguzinYa.E. (1987) *Zhivoi kristall* [Living crystal]. Moscow, Nauka Publ., 192 p. (In Russian)

Goryainov P.M., Ivanyuk E.G. (2010) Energetic percolation, as a reason of self-organization of lithospheric complexes.*"Problemy geologii poleznykh iskopaemykh i metallogenii"*. Mezhdunar. konf. ["Problems of geology of ore deposits and metallogeny". International conference]. Moscow, 205. (In Russian)

Grapes R.H., Keller J. (2010) Fe^{2+}-dominant rhönite in undersaturated alkaline basaltic rocks, Kaisershuhl volcanic complex, Upper Rhine Graben, SW Germany. *Eur. J. Mineral*., **22**, 285-292.

Irving A.J., Frey F.A. (1984) Trace element abundance in megacrysts and their host basalts: constraints on partition coefficients and megacrysts genesis. *Geochim. Cosmochim. Acta*, **48**, 1201-1221.

Johnston A.D., Stout J.H. (1984) Compositional variation of naturally occurring rhönite. *Amer. Mineral*., **70**, 1211-1216.

Kennedy D., Wasserburg G., Heard H., Newton R. (1962) The upper three-phase region in the system SiO_2–H_2O. *Amer. J. Sci*., **260**, 501-521.

Kogarko L., Kurat G., Ntaflos T. (2001) Carbonate metasomatism of the oceanic mantle beneath Fernando de Noronha Island, Brazil. *Contrib. Mineral. Petrol*., **140**, 577-587.

Kowabata H., Hanui T., Chang Q., Kimura J-I., Nichols A.R.L., Tatsumi Y. (2011) The petrology and geochemistry of Saint Helena alkali basalt: evaluation of the oceanic crust-recycling model of HIMU OIB. *J. Petrol*., **52**, 791-838.

Kuo L.C., Kirpatrick R.J. (1985) Dissolution of mafic minerals and its implications for the ascent velocities of peridotite-bearing basaltic magmas. *J. Geol*., **93**, 691-700.

Kutolin V.A., Agafonov L.V., Chepurov A.I. (1976) Relative stability of olivine, pyroxenes, and garnet in basaltic magma and composition of the upper crust. *Dokl. Akad. Nauk*, **321**(5), 1218-1221. (In Russian)

Kyle P., Price R. (1975) Occurrences of rhönite in alkali lavas of the McMurdo volcanic group, Antarctica, and Dunedin volcano, New Zealand. *Amer. Mineral*., **60**, 722-728.

Lang B., Hebeda E., Priem H., Steinitz G., Verdumen E. (1988) K-Ar and Rb-Sr Ages of Early Cretaceous Magmatic Rocks from Makhtesh Ramon, Southern Israel. *Israel J. Earth Sci*., **37**, 65-72.

Lopez M., Pompilio M., Rotolo S.R. (2006) Petrology of some amphibole-bearing volcanics of pre-Ellitico period (102 – 80 ka), Mt. Etna. *Periodico di Mineralogia*, **75**, 151-166.

Messiga B., Bettini E. (1990) Reaction behavior during kelyphite and symplectite formation: a case study of mafic granulites and eclogites from the Bohemian Massif. *Eur. J. Mineral*., **2**, 125-144.

Miller C., Zanetti A., Thoni M., Konzett J., Klotzli U. (2012) Mafic and silica-rich glasses in mantle xenoliths from Wau-en-Namus, Libya: textural and geochemical evidence for peridotite-melt reactions. *Lithos*, **128-131**, 11-26.

Miyashiro A. (1976). *Metamorfizm i metamorficheskie poyasa* [Metamorphism and metamorphic belts]. Moscow, Mir Publ., 535 p. (In Russian)

Nelson S.T., Montana A. (1992) Sieve-textures plagioclase in volcanic rocks produced by rapid decompression. *Amer. Mineral*., **77**, 1242-1249.

Nielson J., Nakata J. (1994) Mantle origin and flow sorting of megacryst – xenolith inclusion in mafic dikes of Black Canyon, Arizona. *US Geol. Surv. Prof. Paper*, **1541**, 41 p.

Ostrovskii N.Yu., Mishina G.P., Povilaitis V.M. (1959) *P-T* projection of SiO_2–H_2O system. *Dokl. Akad. Nauk SSSR*, **126**(3), 645-646. (In Russian)

Rankenburg K., Lassiter J., Brey G. (2004) Origin of megacrysts in volcanic rocks of the Cameron vole: chain-constrains on magma genesis and crustal contamination. *Contrib. Mineral. Petrol*., **147**, 129-144.

Ribbe P. (1960) An X-ray and optical investigation of the peristerite plagioclases. *Amer. Mineral*., **45**, 626-644.

Righter K., Carmichael I.S.E. (1993) Mega-xenocrysts in olivine basalts: fragments of disrupted mantle assemblages. *Amer. Mineral*., **78**, 1230-1245.

Ringwood A.E. (1975) Origin and petrology of the Earth's mantle. *McGraw-Hill*, 618 p.

Samoilov V., Vapnik Ye. (2007) Fractional melting – the determining factor in the origin of thephrite-basanite-nephelinite rock suite: evidence from western Makhtesh Ramon, Israel. *N. Jb. Mineral. Abh.*, **184**(2), 181-195.

Sharygin V.V., Kotai K., Sabo Ch., Timina T.Ju., Terek K., Vapnik Ye., Kuz'min D.V. (2011) Rhönite in alkaline basalts: silicate melt inclusions in olivine phenocrysts. *Geol. Geofiz.*, **52**(11), 1695-1717. (In Russian)

Shaw C.S.J. (1999) Dissolution of clinopyroxene in basanite magma between 0.4 and 0.2 GPa: further implications for the origin Si-rich alkaline glass inclusions in mantle xenoliths. *Contrib. Mineral. Petrol*., **135**, 114-132.

Shaw S.J.S., Eyzaguirre J. (2000) Origin of megacrysts in the mafic alkaline lavas of the West Eifel volcanic field, Germany. *Lithos*, **50**, 75-95.

Shaw S.J.S., Thibault Y., Edgar A.D., Lloyd F.E. (1998) Mechanism of orthopyroxene dissolution in silica-undersaturated melts at 1 atmosphere and implications for the

origin of silica-rich glass in mantle xenoliths. *Contrib. Mineral. Petrol*., **132**, 354-370.

Shubnikov A.V. (1935) *Kak rastut kristally* [How crystals grow]. Moscow; Leningrad, Academy of Sciences of the USSR Publ., 174 p. (In Russian)

Shulze D. (1987) Megacrysts from alkali volcanic rocks. *Mantle xenoliths (ed. P.H. Nixon)*, 443-451.

Snelling A.A. (2007) Rapid ascent of basalts magmas. *Acts and Facts*, **36**, 10.

Stein M., Katz A. (1989) Composition of the subcontinental lithosphere beneath Israel: Inferences from peridotitic xenoliths. *Israel J. Earth Sci*., **38**, 75-87.

Tsuchiyama A. (1985) Dissolution kinetics of plagioclase in the melt of the system diopside–albite–anorthite, and origin of crusty plagioclase in andesites. *Contrib. Mineral. Petrol*., **89**, 1-19.

Tsuchiyama A. (1986) Melting and dissolution kinetics: application to partial melting and dissolution of xenoliths. *J. Geophys. Res*., **91**(B9), 9395-9406.

Upton B.G.J., Finch A.A., Słaby E. (2009) Megacrysts and salic xenoliths in Scottish alkali basalt derivatives of deep crustal and small-melt fractions from upper mantle. *Miner. Mag*., **73**, 943-956.

Vapnik Y. (2005) Melt and fluid inclusions and thermobarometry of mantle xenoliths in Makhtesh Ramon, Israel. *Israel J. Earth Sci*., **54**, 15-28.

Vapnik Y., Sharygin V., Samoilov V., Yudalevich Z. (2007) The petrogenesis of basic and ultrabasic alkaline rocks of western Makhtesh Ramon, Israel: melt and fluid inclusion study. *Inter. J. Earth Sci*., **96**, 663-684.

Villaseca C., Ancochea E., Orejana D., Jeffries T.E. (2010) Composition and evolution of the lithospheric mantle in Central Spain: inferences from peridotite xenoliths from the Cenozoic Calatrava volcanic field. *Petrological evolution of the European lithospheric mantle (Eds M. Coltorti, H. Downes, M. Grégoire, S.Y. O'Reilly)*. Geol. Soc., London, Spec. Publ., **337**, 125-151.

Wang Y., Han B., Griffin W.L., Zhang L., Shu G. (2012) Post-entrainment mineral – magma interaction in mantle xenoliths from Inner Mongolia, Western North China craton. *J. Earth Sci*., **23**, 54-76.

Wilkinson J.F.G. (1975) Ultramafic inclusions and high pressure megacrysts from a nephelinite sill Nandewar Mountains, New Wales, and their bearing on the origin of certain ultramafic inclusions in alkali volcanic rocks. *Contrib. Mineral. Petrol*., **51**, 235-262.

Yudalevich Z.A., Fershtater G.B., Eyal M. (2014) Magmatism of Makhtesh Ramon: geology, geochemistry, petrogenesis (natural reserve of Har Ha-Negev, Israel). *Litosfera*, **3**, 70-92. (In Russian)